Copy of chapter from Perez-Brady book

Hogstrom K.R. Electron beam therapy: dosimetry, planning, and techniques. In: C. Perez, l. Brady, E. Halperin, R Schmidt-Ullrich (eds). Principles and Practice of Radiation Oncology, pp. 252-282, Baltimore; Lippinkott, Williams, and Wilkins, 2003.

CHAPTER 7

ELECTRON-BEAM THERAPY: DOSIMETRY, PLANNING, AND TECHNIQUES

KENNETH R. HOGSTROM

Electron-beam therapy is an important modality at all contemporary radiation therapy clinics. It is readily available in the energy range of 6 to 20 MeV from major accelerator suppliers. Although available for many years using Van de Graf accelerators and betatrons, its utility increased with the availability of linear accelerators in the 1970s.

In 1976 Tapley published one of the earlier, comprehensive treatises on electron radiation therapy (64), in which she stated, "There is no practical way for every radiation therapy department, either in hospitals or private offices, to be equipped with all modalities of irradiation beams. Ideally, electron beams should be available for those clinical situations where electrons are indispensable or very clearly superior." Although electrons are used at most radiation therapy centers, it still might be advantageous to refer patients to regional centers, which offer electron techniques that are used infrequently and require significant experience of the radiation oncologist and technical staff. Special treatment techniques applicable to these conditions will be mentioned later in this chapter.

Since the late 1970s, there have been three developments in electron-beam radiation therapy technology that have improved significantly our ability to deliver electron therapy. First, the advent of computed tomography (CT)-based treatment planning allowed for coverage of the planning target volume (PTV) by the therapeutic dose and the dose to normal tissues and structures to be more accurately assessed. CT also provided a physical description of the anatomy, which is required for accurate dose calculations (15,21). Second, the development of the electron pencil-beam algorithms (PBAs) and their implementation into treatment planning systems in the early 1980s provided a mechanism for accurately calculating dose (17,25,26). Third, manufacturers refined the quality of their electron beams (i.e., depth dose, off-axis uniformity, and penumbral width) by improving dual-scattering foil systems and electron applicators. Presently, the differences in the electron-beam dose characteristics of various radiation therapy machines from different vendors are unimportant when selecting a radiation therapy machine.

Electron-beam therapy is advantageous because it delivers a reasonably uniform dose from the surface to a specific depth, after which dose falls off rapidly, eventually to a near-zero value. The depth of treatment is controlled by selecting the appropriate energy, and when necessary, the bolus thickness. Using electron beams with energies up to 20 MeV allows disease within approximately 6 cm of the surface to be treated effectively, sparing deeper normal tissues.

Electron-beam therapy is useful in treating cancer of the skin and lips, upper-respiratory and digestive tract, head and neck (14,46), breast, and a variety of other sites (37,64,66). Treatment sites of the skin include the eyelids, nose, ear (50), scalp (64,65), and more widely spread diseases of the limbs (e.g., melanoma and lymphoma) (68) or total skin (e.g., mycosis fungoides) (29,31). Treatment sites of upper-respiratory and digestive tract include the floor of mouth, soft palate, retromolar trigone, and salivary glands (14,67). Treatments of the breast include chest-wall irradiation following mastectomy (53,63,64); nodal irradiation, often internal mammary chain and occasionally axillary; and boost to the surgical bed following mastectomy or lumpectomy (55). Other sites of electron-beam therapy include the retina (34), orbit (12), spine (craniospinal irradiation) (10,11,41,42), paraspinal muscles (21,40), pancreas and other abdominal structures (intraoperative therapy) (44), vulva (52), and cervix (intracavitary irradiation) (43).

The purpose of this chapter is to discuss the treatment and treatment-planning techniques necessary to deliver the most effective electron-beam therapy. This requires a basic knowledge of dose distribution in water, dose in the heterogeneous patient, treatment-planning tools and principles, and special techniques using electron beams.

DOSE DISTRIBUTION IN WATER

To appreciate the clinical use of electron beams, their dose distributions in water must be understood. Understanding the properties of depth dose, off-axis ratios, and two-dimensional (2D) isodose contour plots will clarify the concept of dose distribution in water. As well, an understanding of the dependence of the dose distribution on incident energy, field size, and source-to-surface distance (SSD) is required. It usually is assumed that the dose distribution for a specified energy, field size, and SSD is machine dependent but applicator independent. Applicator dependence might have a minor significance in cases where the beam contains a significant number of collimator-scattered electrons; however, in clinical practice applicator dependence is seldom, if ever, accounted for. In contrast, applicator dependence always is considered in the determination of dose output, which is discussed later.

Depth Dose

This section discusses percent dose (values are normalized to 100% at the depth of dose maximum, R_{100}) versus depth in water. Central-axis depth dose implies that the electron field is symmetric about the central axis, and the focus initially will be on square fields. Electron depth dose varies with field size; however, once the field reaches a certain size, side-scatter equilibrium is achieved and further increasing the size has an insignificant effect on depth dose (18,33). In the energy range of up to 20 MeV,

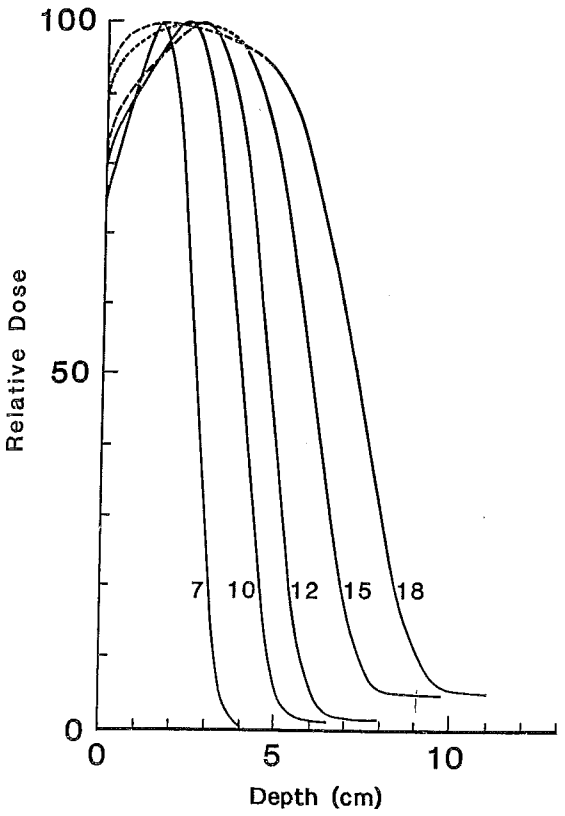

FIGURE 7.1. Energy dependence of depth dose. Plot of relative dose (%) versus depth for a 10 × 10-cm² field size for 7 to 18 MeV beams on a Siemens Mevatron 77 radiation therapy unit (source-to-surface distance, or SSD = 100 cm). (From Meyer JA, Palta JR, Hogstrom KR. Demonstration of relatively new electron dosimetry measurement techniques on the Mevatron 80. *Med Phys* 1984;11:670–677, with permission.)

a 10 × 10-cm² field size typically will achieve side-scatter equilibrium on central axis. The energy dependence of depth dose is illustrated in Fig. 7.1, where central-axis depth dose is plotted for a 10 × 10-cm² field for energies in the range of 7 to 18 MeV. The family of curves illustrates how the dosimetric characteristics vary with the incident electron energy:

1. Surface dose (D_s) increases from approximately 75% to 95% as energy increases from 7 to 18 MeV. The slow increase in dose from the surface to the depth of maximum dose (R_{100}) occurs as a result of electrons undergoing multiple Coulomb scattering in the water (18).
2. Depth of distal 90% (R_{90}), the therapeutic depth, increases as energy increases.
3. Depth of 10% (R_{10}), close to the maximum penetration of the electrons, increases as energy increases.
4. Distance from R_{90} to R_{10} (R_{90-10}), which characterizes the minimum distance that can be placed between tumor (receiving prescribed dose) and critical structure (receiving minimal dose), increases as energy increases;
5. X-ray dose that lies beyond the electron dose component is characterized by its value (D_γ) at the depth of the practical range (R_p), and it increases as energy increases.
6. The R_{100} depth can vary irregularly with depth and model of electron treatment machine; its dependence is insignificant for treatment planning, although it is significant to the medical physicist for constructing percent depth-dose data and in beam calibration.

Depth dose has a significant dependence on field size, and the dependence varies with incident electron energy. The primary reason for the field-size dependence is loss of side-scatter equilibrium, which has been discussed in detail by Hogstrom and colleagues (18,33). Figures 7.2A and 7.2B, which show the field-size dependence of percent depth dose at 9 and 20 MeV, clearly illustrate that it is a greater issue at the higher energies. Loss of side-scatter equilibrium, which begins first at the deeper depths, results in R_{90} shifting toward the surface as field size decreases. The shift also increases the R_{90-10} distance, as R_{10} changes only slightly. As the field size gets even smaller, the maximum dose decreases, and when it is normalized to 100%, the relative dose at the surface, D_s, increases. Also, the effects on the distal portion of the depth-dose curve are greater. The most clinically significant effect is the decrease in R_{90} with decreasing field size, which can require a greater energy than thought for treatment using small fields.

Depth-dose variations with SSD are usually insignificant. Differences in the depth dose resulting from inverse square effect are small because electrons do not penetrate that deep (6 cm or less in the therapeutic region) and because the significant growth of penumbra width with SSD restricts the SSD in clinical practice to typically 115 cm or less. The primary effect of inverse square is that R_{90} penetrates a few millimeters deeper at extended SSD at the higher energies, as illustrated in Fig. 7.3. In relatively few cases (e.g., when the electron beam has a large component of collimator-scattered electrons) the variation in depth dose with SSD can become more significant. In such cases the collimator-scattered electrons are scattered out of the beam, resulting in a depth dose with a lower D_s and greater R_{90} (60).

Depth-dose curves will vary between treatment machines of different design, even for exactly the same beam energy. However, the differences for modern day radiation therapy accelerators are minimal and should not be a major factor when deciding which accelerator would best meet a clinic's needs.

For rectangular fields, Hogstrom and colleagues (25) derived and many have confirmed (25,45,60) that percent depth dose can be calculated by taking the geometric mean of the percent depth doses for a square field of length dimension (L) and one of width dimension (W). That is,

$$\%D(d; L \times W) = \sqrt{\%D(d; L \times L) \cdot \%D(d; W \times W)}. \qquad (7.1)$$

If the square field, percent depth-dose curves do not have a common R_{100}, then the result of equation 7.1 must be normalized such that its maximum equals 100%. This method is referred to as the *square-root method.*

In some instances (e.g. intraoperative, intraoral, or intravaginal cones) circular fields are used. In such cases, it will be necessary to measure their dose distributions independent of those determined for square or rectangular fields.

Usually, a collimating insert is placed inside an electron applicator to form an irregularly shaped field, occasionally blocking the central axis. In such cases, central-axis depth dose makes little sense, and the term "central-field depth dose" should be used, providing that the field has an axis of symmetry. In cases

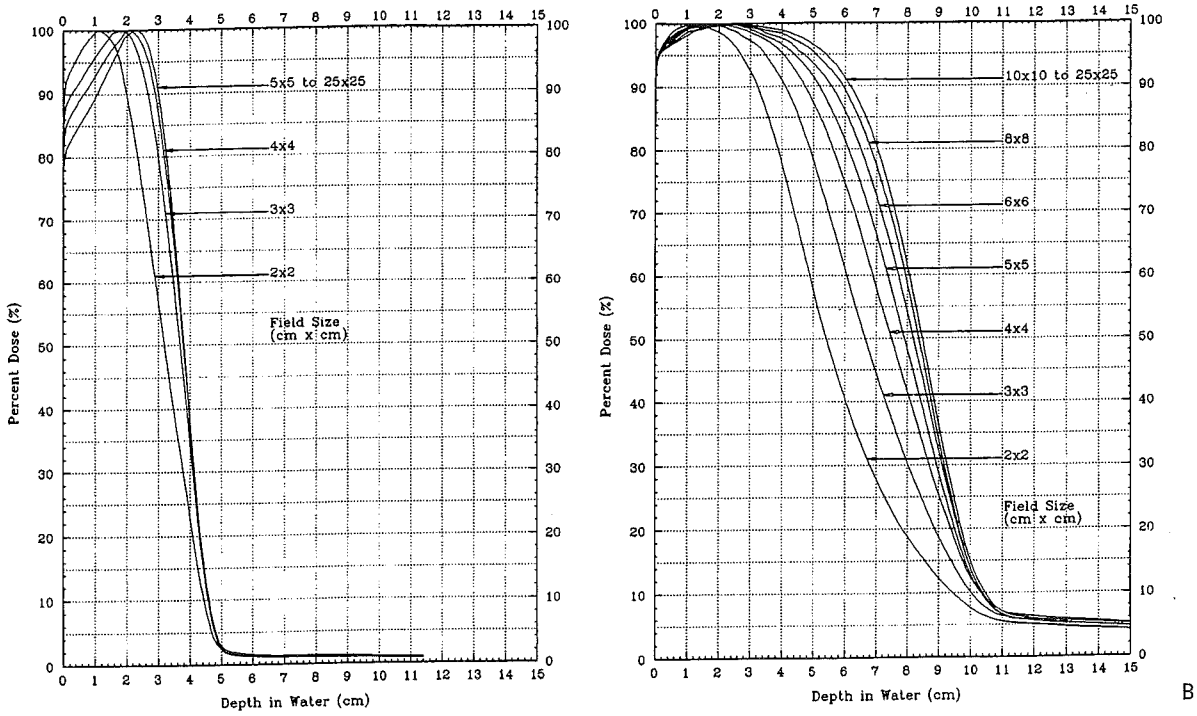

FIGURE 7.2. Field-size dependence of depth dose. Plot of percent dose versus depth for field sizes from 2 × 2 to 25 × 25-cm² for **(A)** 9-MeV and **(B)** 20-MeV beams on a Varian Clinac 2100C radiation therapy unit (source-to-surface distance, or SSD = 100 cm).

where the insert is irregular, the depth dose can be approximated using a rectangularly shaped field that approximates the irregularly shaped field (28). In highly irregular-shaped fields, the dose distribution can be calculated in water or in the patient using an appropriate dose algorithm in a three-dimensional (3D) treatment-planning system.

Off-Axis Dose

Dose distributions in the dimensions perpendicular to the central axis can be described by off-axis ratios. The off-axis ratio (OAR) is defined as the ratio of dose at an off-axis position to that on the central axis at the same depth. Off-axis ratios measured in water are used to assess off-axis beam quality, which is characterized by flatness and symmetry in the uniform portion of the beam and by its fall-off in the region of the penumbra (e.g., 90%–10%, W_{90-10}).

Manufacturers should be able to provide electron beams with a symmetry specification of 2% for opposing points in the beam and a flatness specification of ± 3% *of the central-axis value* along the major axes (± 4% along diagonals). American Association of Physicists in Medicine (AAPM) Task Group 25 recommended

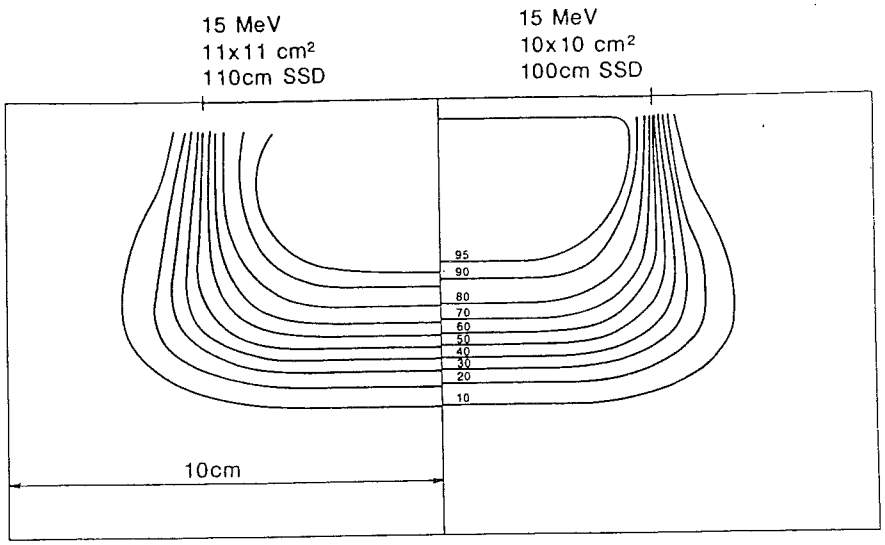

FIGURE 7.3. Source-to-surface distance (SSD) dependence of depth dose. Comparison of isodose plots for 15-MeV beam, 10 × 10-cm² at 100-cm SSD with 11 × 11-cm² field at 110-cm SSD. (From Hogstrom, KR. Clinical electron beam dosimetry: basic dosimetry data. In: Purdy JA, ed. *Advances in Radiation Oncology Physics: Dosimetry, Treatment Planning, and Brachytherapy.* Woodbury: American Institute of Physics, Inc.,1991:390–429, with permission.)

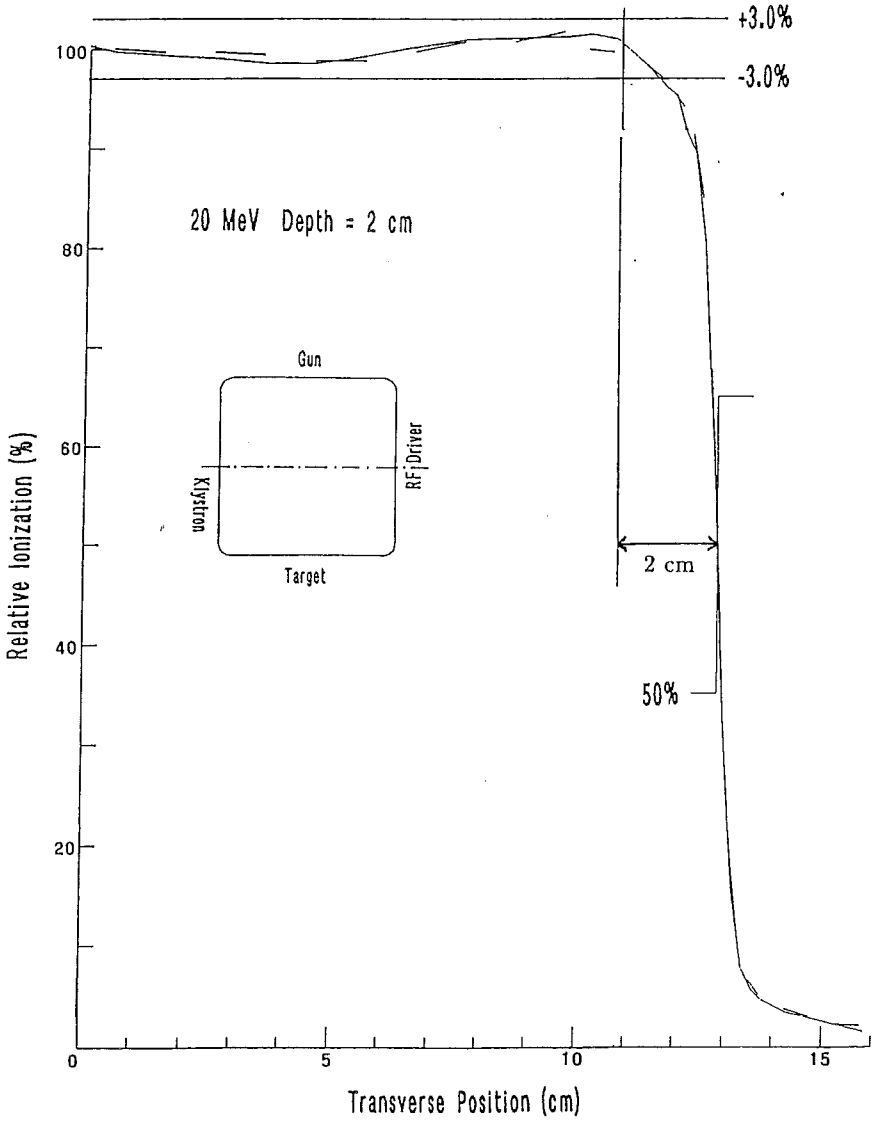

FIGURE 7.4. Beam uniformity verification. Plot of off-axis ratios versus position along a major axis. Data having a negative position (*dashed curve*) is reflected about central axis for comparison with data having a positive position (*solid curve*). Data measured at a depth of 2 cm in water at 100-cm SSD for a 20-MeV beam (Varian Clinac 2100C, 25 × 25-cm^2 open applicator).

that flatness and symmetry should be evaluated along major axes (lines containing central axis and perpendicular to the collimator edges) and along diagonal axes (33). Task Group 25 also recommended that flatness and symmetry be evaluated at depths near the surface and therapeutic depth. However, I only recommend the former, specifically a depth of 1 cm for energies of 9 MeV and less and a depth of 2 cm for energies greater than 9 MeV. Flatness and symmetry are evaluated inside the penumbra, which usually is assured by setting the boundaries of evaluation 2 cm inside the collimating edge ($2\sqrt{2}$ cm along diagonals). The medical physicist should prescribe electron-beam flatness and symmetry specifications for new radiation therapy machines and should measure performance as part of the machine-acceptance procedure for all energy and applicator combinations. Fig. 7.4 shows the result for a typical accelerator performance evaluation.

Penumbra of electron beams are predetermined by the design of the beam flattening system, the air gap between the final collimator, and the scatter of electrons in water. Penumbra, a function of depth, is the root mean square addition of two penumbral components, one the result of the air gap and one the result of scatter in the water (17,25). This dependence is complex, but can be appreciated qualitatively by the illustration in Fig. 7.5, which compares isodose plots for normal (100 cm) and extended (110 cm) SSD at 6 and 16 MeV. These data show that penumbra grows in a nonlinear fashion with depth, that air gap is more significant at the lower energies, and that scatter in water dominates at the higher energies. Fortunately, the complex dependence of penumbra can be modeled accurately in treatment-planning systems using the pencil-beam or more sophisticated dose algorithms (17,25,26,27).

Isodose Plots

Combining depth dose with off-axis ratios results in the 3D dose distribution, and the properties of the 3D dose distribution can be appreciated by viewing 2D isodose contour plots in a plane containing the central axis and a major axis. Examples of these plots for a 15 × 15-cm^2 field are illustrated in Fig. 7.5. As field width decreases or increases, the penumbra shape changes insignificantly; it simply slides in or out, respectively.

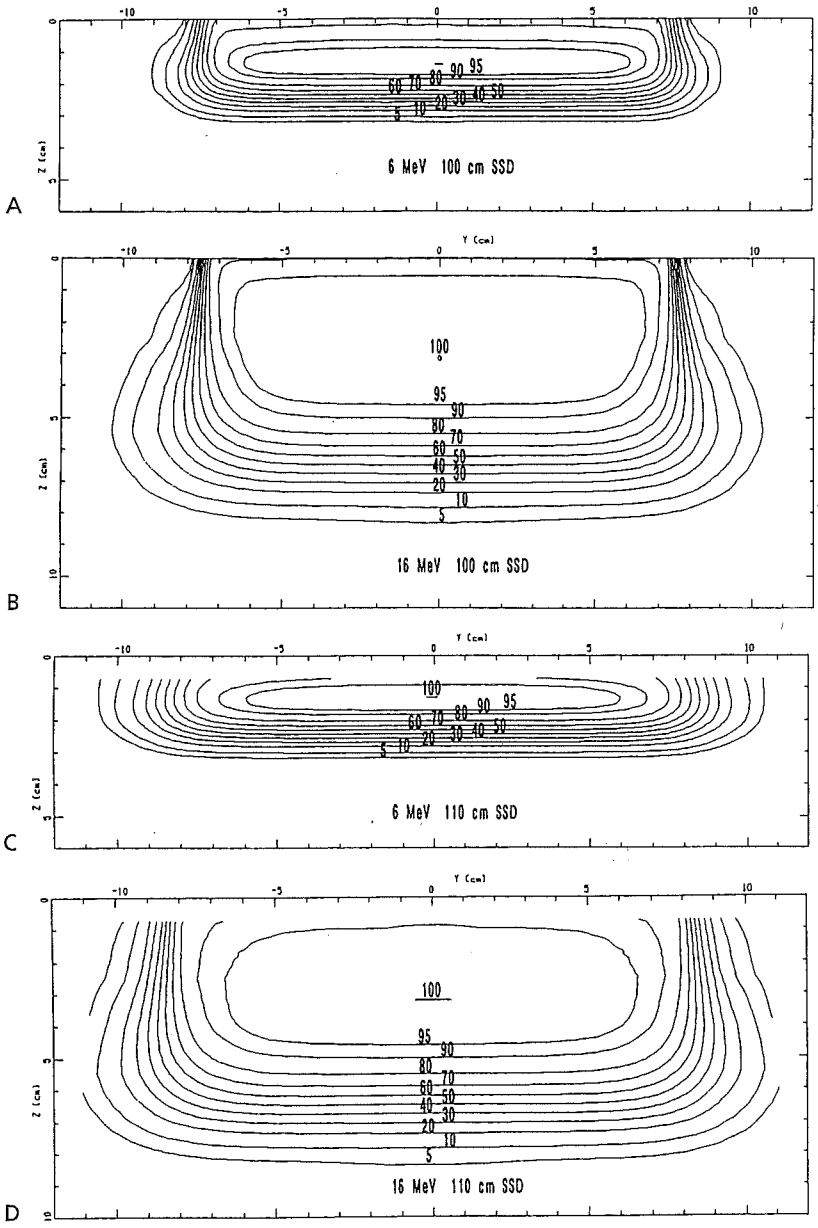

FIGURE 7.5. Variation of dose distribution with energy and SSD. Isodose plots (5% to 100%) in water for open 15 × 15-cm^2 applicator and for **(A)** 6 MeV, 100-cm SSD, **(B)** 16 MeV, 100-cm SSD, **(C)** 6 MeV, 110-cm SSD, and **(D)** 16 MeV, 110-cm SSD (Varian Clinac 2100C).

Data required for isodose contours are acquired for an inclusive spread of field sizes at each energy. 2D isodose contour plots and data are useful for manual treatment planning, input data required by dose algorithms, verification of dose calculated by a treatment-planning system, and quality assurance standards (18,33).

DOSE IN THE HETEROGENEOUS PATIENT

For most clinical circumstances, the ideal irradiation condition is for the electron beam to be incident normal to a flat surface with underlying homogeneous soft tissues. The dose distribution for this condition, similar to that for a water phantom described previously, contains a reasonably uniform dose inside the penumbra from the surface to R_{90}, and it has the sharpest possible fall-off laterally and with depth. As the angle of incidence deviates from normal, as the surface becomes irregular, and as internal heterogeneous tissues (e.g., air, lung, and bone) become present, the qualities of the dose distribution degrade (16). Internal heterogeneities can change the depth of beam penetration as a result of differences in the rate of energy loss, which can result in PTV underdose and critical structure overdose. Both irregular surfaces and internal heterogeneities create changes in side-scatter equilibrium, producing volumes of increased dose (hot spots) and decreased dose (cold spots). These changes appear in a region downstream of the lateral boundary of the heterogeneity, which can result in increased dose to normal tissues and critical structures and decreased dose to the PTV (16,21). In such cases, the hot spots lie under the less dense of the unit density and heterogeneous tissues. These effects, if known, often can be reduced or eliminated by modifying the treatment technique.

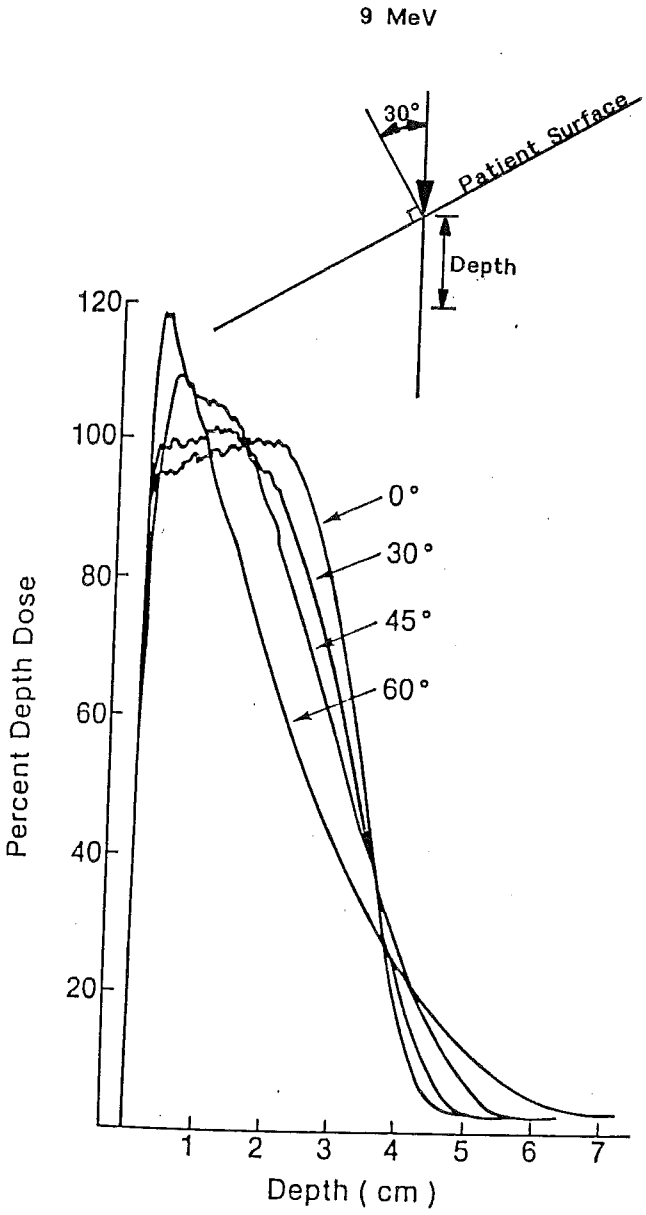

FIGURE 7.6. Effect of angle of incidence on depth dose. Dose versus depth for a 9-MeV beam incident on water angled 0°to 60° from the normal. (From Ekstrand KE, Dixon RL. The problem of obliquely incident beams in electron-beam treatment planning. *Med Phys* 1982;9:276–278, with permission.)

Irregular Surfaces

Two geometries that illustrate the effects on the dose distribution caused by an irregular patient surface are the sloped skin surface and the stepped skin surface. Figure 7.6, illustrates changes in the depth-dose curve as a result of nonnormal incidence of an electron beam onto a flat surface. Compared with normal incidence, the nonnormal incident, central-axis, depth-dose curve shows: (a) an increased surface dose, (b) an increased dose maximum, (c) a decreased penetration of the therapeutic dose (R_{90}), and (d) an increased range of penetration (13,33). These changes can be clinically significant, particularly at angles of incidence greater than 30° from the normal. Such conditions can occur when irradiating curved patient surfaces with large fields (e.g., chest wall, limbs, neck, and scalp). Also, it should be appreciated that the depth of R_{90} is specified along the central axis of the beam, and if the depth is taken perpendicular to the surface, then the depth is further reduced (approximately) by the factor cos (θ), where θ is the deviation of the incident angle from the normal. These data explain why the lateral chest wall cannot be irradiated using an anterior beam—the surface dose would be too great and the penetration would be too little.

Any time a sharp gradient (stepped surface) occurs on the patient's surface, side-scatter equilibrium will be lost, resulting in a cold spot beneath the proximal surface and a hot spot beneath the distal surface (7,16,19,59). This can occur as a result of a bolus edge, surgical defects, or normal anatomy. For example, in the use of uniform thickness bolus that partially covers a field, a 90° edge can result in hot or cold spots as great as 20%, as illustrated in Fig. 7.7. In such a case, the bolus should be tapered as much as possible; the results of the 45° tapered bolus in Fig. 7.7 show a reduction in the hot spot but, more significantly, an increased coverage of the 90% isodose contour. The nose is a protrusion that creates a cold spot beneath itself, often the location of the tumor (16,19,26). The ear canal (Fig. 7.8) and surgical voids, which are characterized by a depression in the patient's surface, can result in hot spots in excess of 50% beneath, depending on their dimensions and the beam energy (50,54). Such depressions normally should be filled with some type of bolus material. Normal anatomy contains many irregular surface depressions and protrusions (e.g., the ear canal and the nose, respectively). Their effect must be considered in treatment planning.

Air Cavities

The influence of an internal air cavity is illustrated in Fig. 7.9, which compares isodose contours beneath an air cavity to those without the air cavity. Results show that: (a) the isodose contours in the shadow of air are shifted distally, (b) the dose beneath the air cavity increases as a result of loss of side-scatter equilibrium, and (c) the influence of the air increases laterally with depth. Internal air cavities of clinical interest primarily occur in treatment of the head and neck (e.g., nasal passages, ethmoid sinuses, maxillary sinuses, larynx, and mastoids) (16,19).

Another significant effect is the reduction in dose in unit density tissue lateral to an air cavity. Electrons scattering from the unit density tissue into the air are not replaced because air is unable to scatter an equal amount back into the unit density tissue. Figure 7.10 shows the example of the nasal septum receiving a dose approximately 10% less than that expected assuming the patient is water. Frequently, nose tumors can spread into the septum, in which case bolus should be used to eliminate or reduce underdosing.

Lung

In lung, electrons can penetrate three to four times further than in unit density tissue. This is demonstrated in Fig. 7.11, where isodose contours from a typical electron chest wall treatment are compared with those in which the lung is assumed unit density. Assuming a given dose of 50 Gy, the 40% isodose contour

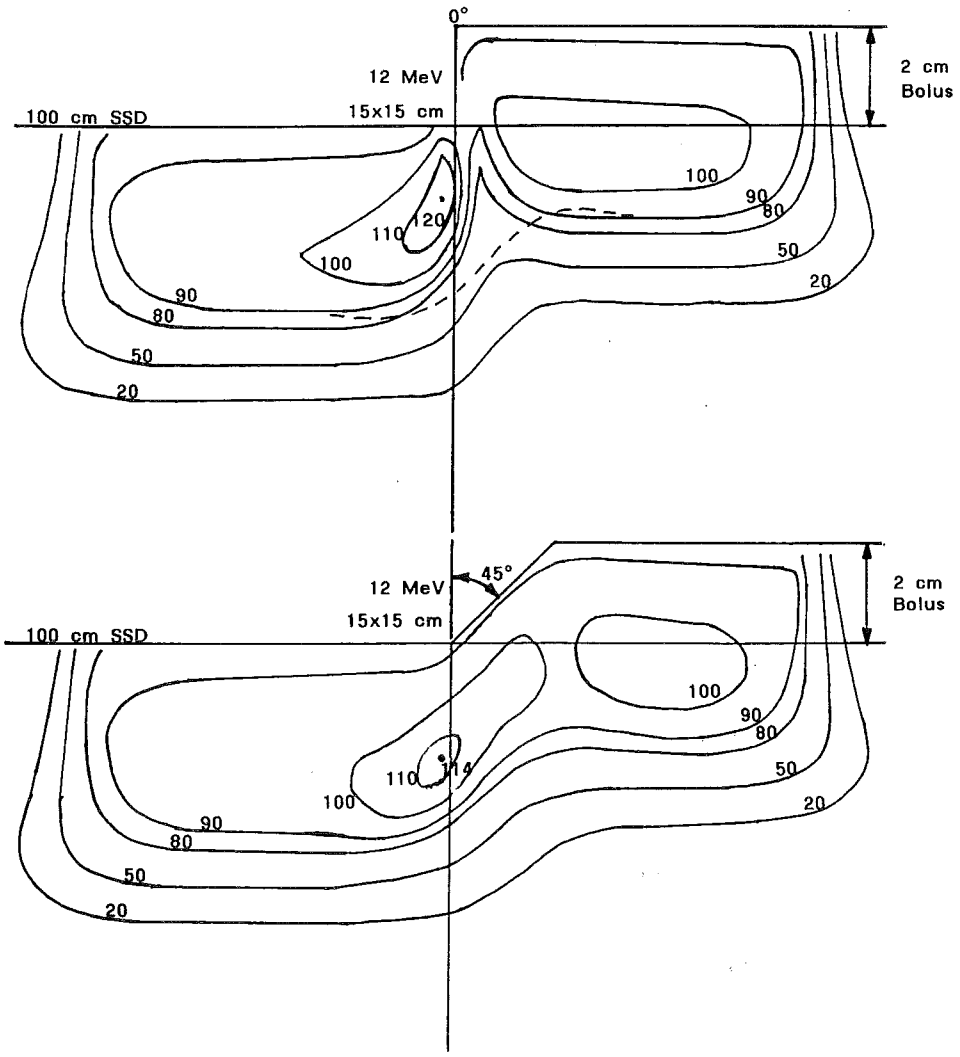

FIGURE 7.7. Effect of irregular patient surface on dose distribution. Plot of isodose contours for a 12-MeV, 15 × 15-cm² beam incident on water at 100-cm source-to-surface distance (SSD) having a stepped surface resulting from a 2-cm slab of bolus **(top)** and a beveled edge (45°) on the stepped surface **(bottom)**. The dashed line in the top figure shows the location of the 90% isodose contour in the bottom one. (From Hogstrom KR. Treatment planning in electron beam therapy. In: Vaeth JM, Meyer JL, eds. *Frontiers of Radiation Therapy and Oncology Vol. 25: The Role of High Energy Electrons in the Treatment of Cancer.* Basel: S. Karger AG, 1991:30–52, with permission.)

corresponds to 20 Gy, approximately the threshold for pneumonitis. Ignoring the low density of lung would grossly underestimate the volume of lung above 20 Gy (19).

This effect can be even more significant because of the large gap between adjacent energies found on most radiation therapy accelerators (3 to 4 MeV). For example, increasing the beam energy from 9 to 12 MeV results in an additional 1.5 cm of penetration in waterlike tissue (electrons lose energy at a rate of approximately 2 MeV/cm in water), and this corresponds to as much as 6.0 cm in lung (assuming a lung density of 25%). Consider the patient whose chest wall thickness requires an energy of 10 MeV for treatment and that 12 MeV must be selected. This results in as much as 4 cm in depth of needless irradiation in lung, unless 1 cm of bolus is used to effectively lower the energy incident on the patient to 10 MeV.

Bone

The influence of bone is illustrated in Fig. 7.12, which compares isodose contours beneath hard bone to those without the bone. The results show that: (a) the isodose contours in the shadow of the bone are shifted proximally, (b) dose outside (inside) the bone-water interface increases (decreases) by approximately 5% as a result of loss of side-scatter equilibrium, and (c) the lateral dimension of the region having its dose perturbed by the bone increases with depth. Actual bones are not uniformly dense throughout their cross-section, and in most cases their edges are not parallel to the incident beam. Both differences decrease the influence of bone in generating inhomogeneity in the patient's dose distribution. Dense bones that significantly affect the dose distribution include the mandible, bones of the skull (e.g., frontal bone and zygoma in orbit treatment or temporal bone in treatment of parotid), clavicles, and vertebral processes (e.g., craniospinal irradiation). Figure 7.13 compares the calculated dose distribution for 18-MeV electrons irradiating carcinoma of the left buccal mucosa and retromolar trigone with that calculated assuming the patient was water. Most significantly, the 90% isodose contour is shifted toward the surface because of the mandible. Less significantly, a hot spot in excess of 100% is observed anteriorly and medially from the mandible.

Another question that occasionally arises is, "What is the clinical significance of the increase in dose in or around bone due to increased scatter?" The maximum dose increase expected as a result of backscattered electrons is 5%, and the maximum dose increase expected inside bone and in adjacent exit tissues is approximately 7% (56). These increases represent maximum dose estimates

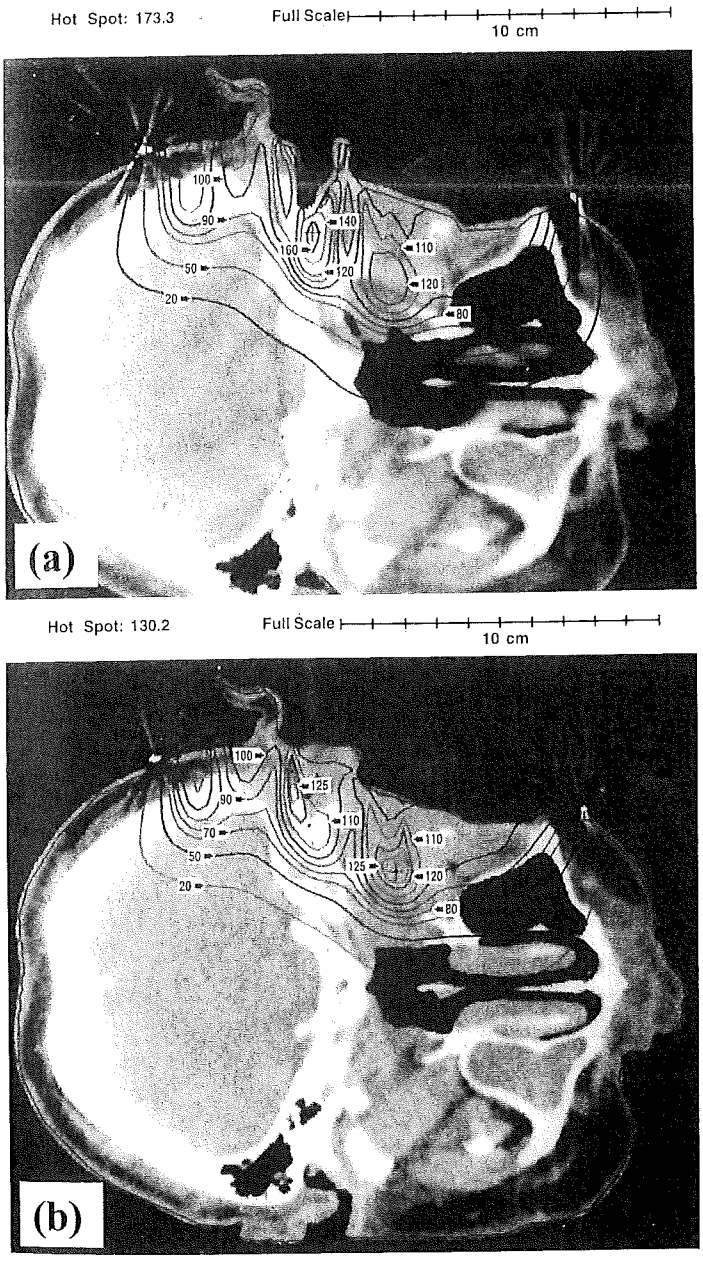

FIGURE 7.8. Impact of irregular surface anatomy on dose distribution. A 15-MeV electron beam irradiates the left side of a patient treated for dermal squamous carcinoma with perineural invasion. A beeswax bolus protects the posterior cranial fossa and the maxillary sinus. Isodose contours, expressed as a percent of given dose, show **(a)** how the ear canal results in an unacceptable hot spot of 160% to the middle ear and **(b)** how filling the ear canal with bolus (saline solution) eliminates that hot spot. The residual hot spot of 125% is a result of the external ear. (From Morrison WH, Wong PF, Starkschall G, et al. Water bolus for electron irradiation of the ear canal. *Int J Radiat Oncol Biol Phys* 1995;33:479–483, with permission.)

because actual bones are not as dense through and through as are the bone substitute in which these data were taken. These estimates of the increased dose are not expected to be clinically significant. In fact, untoward effects in or around bone that can be attributed to dosimetry have not been observed in patients treated with electron-beam therapy.

DOSE PRESCRIPTION AND CALCULATION OF MONITOR UNITS

Dose Prescription

It is recommended that dose be prescribed to given dose or 90% of given dose. Given dose is defined as the maximum central-axis dose in a water phantom at the SSD of the patient for the energy, applicator, and field size identical to that used for patient treatment. If the field shape is irregular, then the field size is taken to be a rectangular field representative of the irregular field shape. The most representative rectangular field is not well defined; however, Hogstrom and associates (28) have provided one methodology for determining its estimate.

It is recommended that dose be prescribed to given dose or a percentage of it and not to a point in the patient. It is quite possible that a dose prescription point in the patient could be in a region of increased or decreased dose because of tissue heterogeneity or irregular surface, which could result in PTV underdose or overdose, respectively.

Calculation of Monitor Units

Monitor units can be determined by

$$MU = \frac{D_{prescribed}/\%D}{O(E,C,LxW,SSD)}, \qquad (7.2)$$

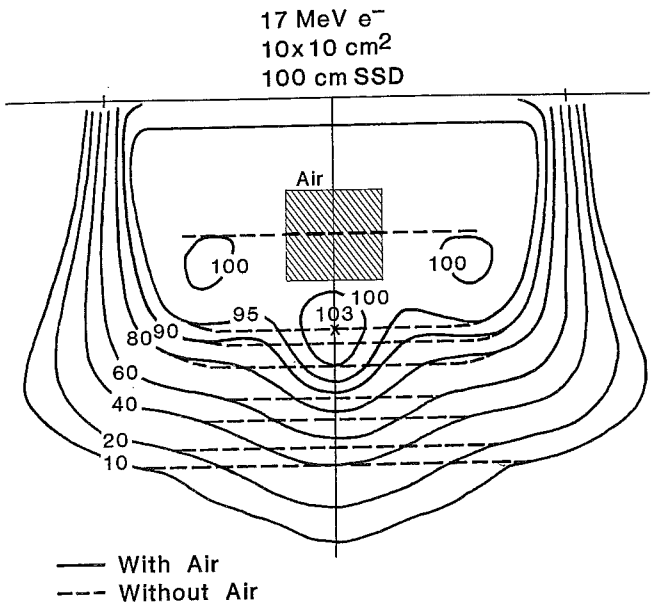

FIGURE 7.9. Effect of internal air cavity on underlying dose distribution. Dose calculated by the pencil-beam algorithm (PBA) for a 2 × 2-cm² cylinder of air located 2 cm below the surface in water is compared to that in its absence. (From Hogstrom KR. Dosimetry of electron heterogeneities. In: Wright AE, Boyer AL, eds. *Advances in Radiation Therapy Treatment Planning*. New York: American Institute of Physics, Inc., 1983:223–243, with permission.)

where $D_{prescribed}$ is the prescribed dose, $\%D$ is the percent of given dose to which dose is prescribed (e.g., 90%), and $O(E,C,LxW,SSD)$ is the output (dose per monitor unit) for a beam of energy E, applicator C, field size LxW, and SSD. To use this methodology, the medical physicist must measure dose output as a function of square field size and SSD for each energy-applicator combination at the time of commissioning the accelerator. Output for rectangular fields can be determined using the *square-root method* of Hogstrom (48,49,60),

$$O(E,C,LxW,SSD) = [O(E,C,LxL,SSD)\cdot O(E,C,WxW,SSD)]^{1/2}. \quad (7.3)$$

Output for rectangular fields also can be determined using an equivalent square method (5,32,33,45); however, Biggs and associates (5) recommends limiting this method to an aspect ratio ($L:W$) of 2:1. The square-root method is not limited to the aspect ratio, and Shiu and colleagues (60) have shown it to be more accurate. Figure 7.14 illustrates beam output data at 9 MeV for four common applicators used on the Varian Clinac 2100C Varian Medical Systems, Palo Alto, CA) at 100 cm SSD.

Output at extended SSD can be determined by either the air-gap method or the effective-source method (33). The effective-source method is covered in detail by Khan (32). The air-gap method has a sounder physical basis. Although both methods give similar answers, only the air-gap method will be covered here (45). Output at extended SSD is given by the product of output at the nominal SSD (SSD_0), the air-gap factor

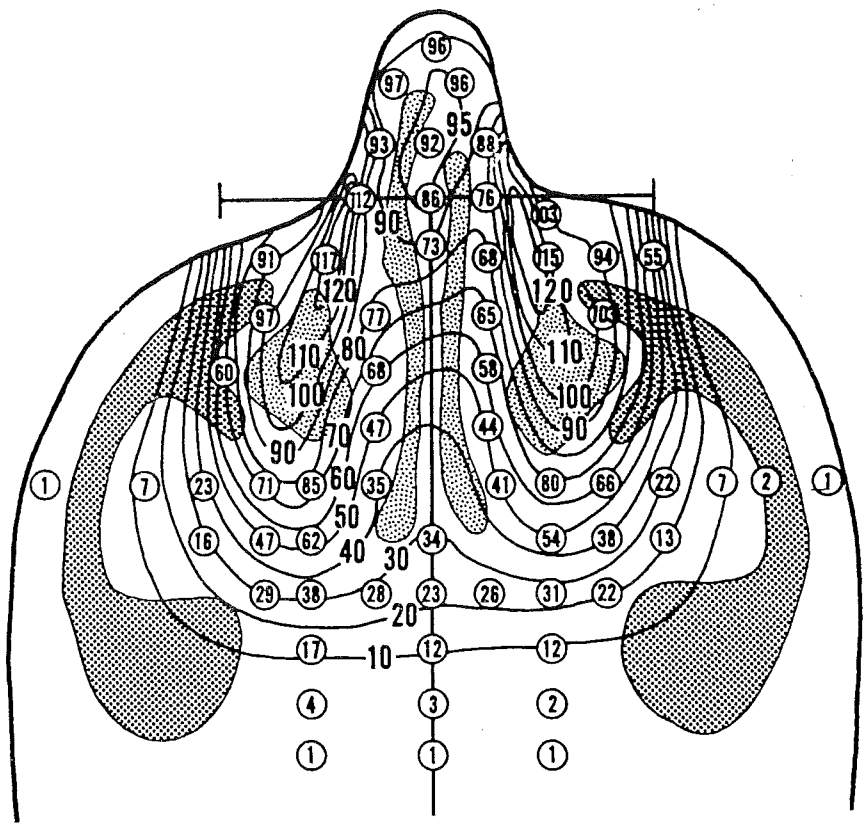

FIGURE 7.10. Effect of nasal cavities to septum. Comparison of dose calculated by the pencil-beam algorithm (*isodose contours*) with thermoluminiscence dosimetry-measured dose (*circled numerical values*) in a two-dimensional phantom designed from a transverse computed tomography slice of a patient with a carcinoma invading the nasal septum (13 MeV, 8 × 8-cm² beam, source-to-surface distance, or SSD = 100 cm). (From Hogstrom KR, Mills MD, Meyer JA, et al. Dosimetric evaluation of a pencil-beam algorithm for electrons using a two-dimensional heterogeneity correction. *Int J Radiat Oncol Biol Phys* 1984;10:561–569, with permission.)

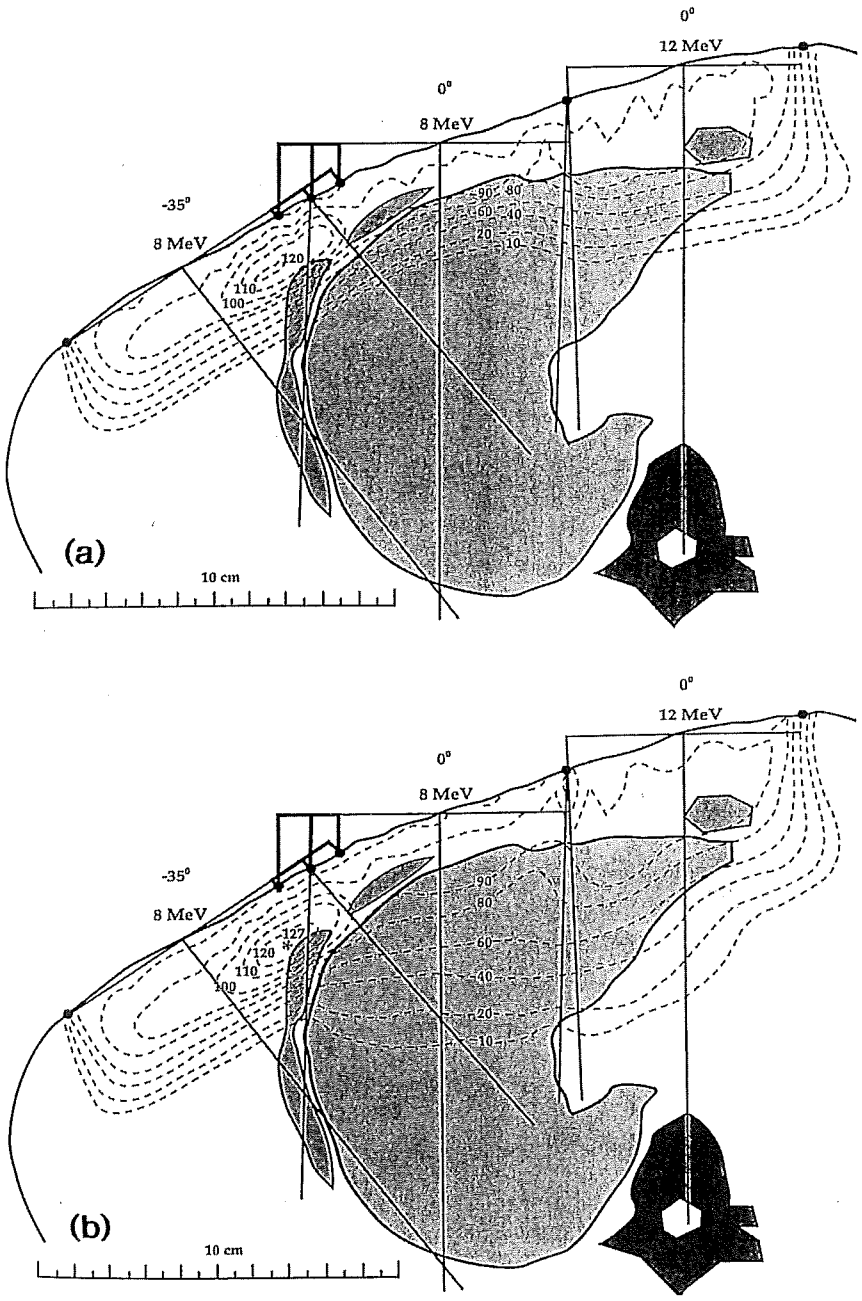

FIGURE 7.11. Effect of lung on dose distribution underlying chest wall. Comparison of dose calculated by the pencil-beam algorithm (PBA) for 8-MeV chest-wall irradiation, assuming **(a)** patient is water and **(b)** heterogeneous anatomy based on computed tomography data.

(fair), and an inverse square term,

$$O(E,C,LxW,SSD) = O(E,C,LxW,SSD_0)\cdot f_{air}(E,LxW,SSD)\cdot \left(\frac{SSD_0 + R_{100}}{SSD + R_{100}}\right)^2. \quad (7.4)$$

f_{air} is determined by measuring dose output for square fields at the extended SSD and then solving equation 7.4. For rectangular fields, the air gap factor is determined using the square-root method (60),

$$f_{air}(E,LxW,SSD) = \sqrt{f_{air}(E,LxL,SSD)\cdot f_{air}(E,WxW,SSD)}. \quad (7.5)$$

As f_{air} is assumed independent of applicator, the dose output needs to be measured only for the smallest applicator that contains the square field size. Figure 7.15 plots the square field air gap factors for the 9-MeV beam of the Varian Clinac 2100C for SSD from 100 to 120 cm. For a more detailed explanation of dose output and sample calculations of monitor units for electron beams, refer to Hogstrom and colleagues (28).

CALCULATION OF DOSE IN PATIENT

Standards for Patient Dose Calculations

Sound treatment-planning decisions require accurate dose calculation in the patient. Therefore, the following recommendations

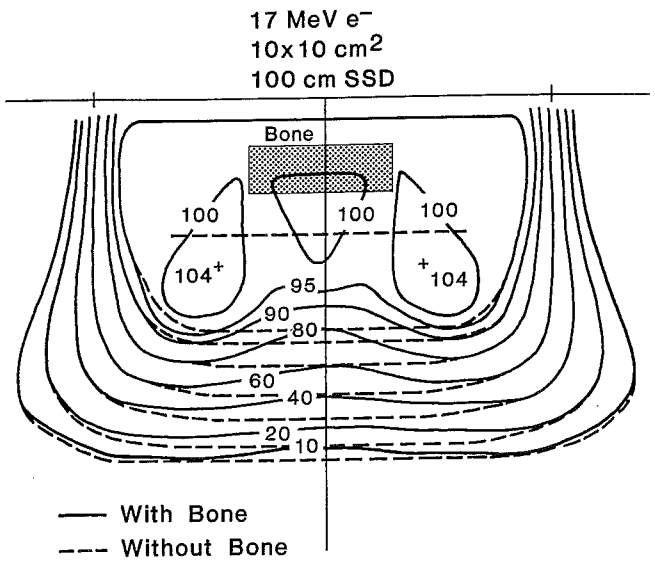

FIGURE 7.12. Effect of hard bone on underlying dose distribution. Dose calculated by the pencil-beam algorithm (PBA) for a 3 × 1-cm² cylinder of hard bone substitute located 1 cm below the surface in water is compared to that in its absence. (From Hogstrom KR. Dosimetry of electron heterogeneities. In: Wright AE, Boyer AL, eds. *Advances in Radiation Therapy Treatment Planning.* New York: American Institute of Physics, Inc., 1983:223–243, with permission.)

are made for electron-beam treatment planning. First, dose should be calculated in the full three dimensions to allow for evaluation of dose homogeneity in the PTV, coverage of the PTV by the 90% dose contour, and dose to critical structures. Second, the dose algorithm should account for patient heterogeneity. Failure to properly account for patient heterogeneity can result in failure to appreciate dose heterogeneity, PTV underdose, or normal-tissue overdose (16,19,21). Third, the dose algorithm should be accurate, and those conditions for which this is not the case should be understood to allow proper interpretation of the dose calculations.

To expand on the final recommendation, a dose algorithm must meet certain criteria to be most effective in the clinic (27). First, it should be accurate to within 4% in regions of low-dose gradients or within 2 mm in regions of high-dose gradient (e.g., penumbra or depth-dose fall-off region). Second, the dose algorithm should be commissioned easily by a qualified medical physicist. Third, the accuracy of the dose algorithm should be well documented. Since 1981, the PBA has best met this requirement. Presently, several new, more accurate algorithms, both analytical and Monte Carlo-based, are being implemented into commercial treatment-planning systems and will replace or supplement the PBA in due time. Regardless of the algorithm, it is the medical physicist's responsibility to commission the algorithm, to understand its accuracy, and to train medical dosimetrists and radiation oncologists in its use.

Additionally, the treatment-planning system and electron-beam algorithm should be integrated and sufficiently functional to allow the treatment planner to simulate the method in which the patient actually is treated. Presently, most systems allow irregular fields, arbitrary SSD, and constant-thickness bolus. However, many do not model individual applicators nor calculate absolute dose (i.e., dose per monitor unit). Few if any allow for skin collimation, arc therapy, or variable thickness bolus. Incorporating these features is well within the capability of today's technology but will not be made available until radiation oncologists hold the treatment-planning system manufacturers accountable.

Dose Algorithms

For the past 20 years, the standard methodology for dose calculation in the patient has been the PBA. Various versions have been implemented into commercial treatment-planning systems, and many are based on the Hogstrom algorithm (25,26). As computing power increased, it was possible to implement the algorithms into 3D format (62). Detailed instructions for commissioning the dose algorithm and documentation of its accuracy have been published (17,26,27). The PBA has been shown to be quite accurate in water at standard and extended SSD, correctly predicting the changes in penumbra (25,26,27). It is also quite accurate in predicting changes in dose resulting from oblique incidence and irregular surfaces (26,27). Regarding internal heterogeneities, it correctly predicts the penetration in lung and the growth of the penumbra width in lung (25,27); however, it tends to underestimate the dose in lung near the mediastinum as a result of its central axis approximation (27). In bone, it correctly predicts the shortening of the dose penetration behind the bone, and it slightly underestimates (<5%) the magnitude of the hot and cold spots under the edge of a thick, hard bone such as the mandible (26). The PBA does not predict the increased dose (<5%) resulting from backscatter at the proximal tissue-bone interface, nor does it predict the increased dose (>7%) in bone resulting from increased scatter. The PBA does a reasonably good job of predicting the increase in penetration behind air cavities; however, it underestimates the hot and cold spots under the air-tissue interfaces (26,27). Figure 7.10 demonstrates the accuracy of the PBA calculation of dose for irradiation of a nose tumor. The dose in the fall-off region is sufficiently accurate; however, the dose in the septum adjacent to the nasal passages is overestimated by as much as 13%, which could impact a treatment outcome if not realized. Usually, the PBA is not subjected to such stringent conditions for dose calculation because proper treatment planning uses methods to avoid poor dose distributions, as illustrated here.

New dose algorithms that are accurate to 4% or better are becoming available in commercial treatment-planning systems. Many of these algorithms have been reviewed by Hogstrom and colleagues (27). One of these is the pencil-beam redefinition algorithm (PBRA), whose commissioning is similar to that of the conventional PBA, although its accuracy is significantly improved (8,9,57). Figure 7.16 illustrates the improvement of the PBRA. Many of the newer algorithms are based on Monte Carlo methods, which allow them to be quite accurate. Precision, resolution, time of calculation, documentation of dose accuracy, and ease of beam commissioning remain issues that must be demonstrated before Monte Carlo-based algorithms can become routinely used, although these issues are being addressed actively by researchers.

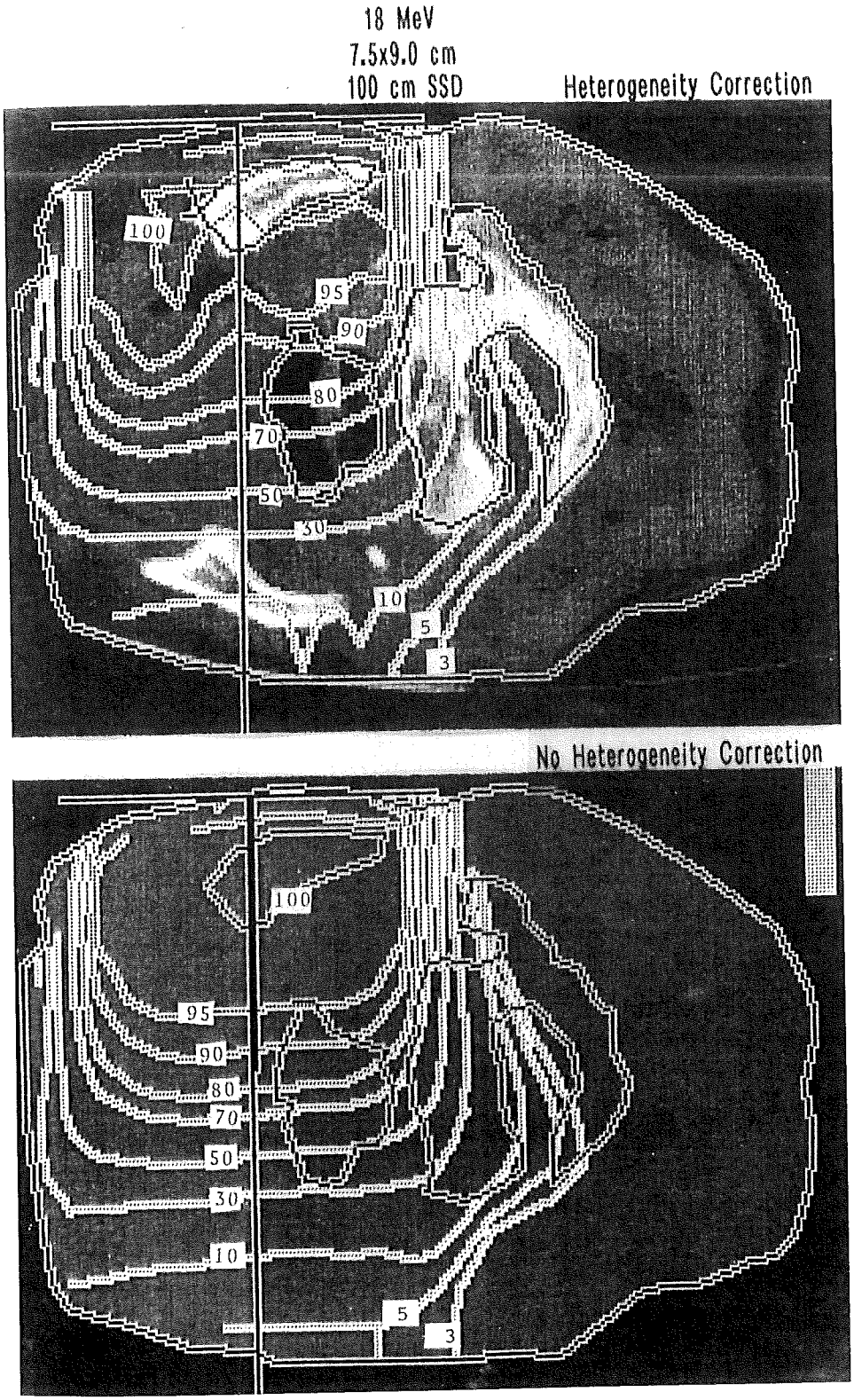

FIGURE 7.13. Effect of mandible in irradiation of retromolar trigone. Dose distributions from an 18-MeV beam that were calculated using a two-dimensional (2D) implementation of the Hogstrom pencil-beam algorithm (PBA) assuming patient is water **(lower)** and accounting for 2D heterogeneity of patient **(upper)**. (From Hogstrom KR. Treatment planning in electron beam therapy. In: Vaeth JM, Meyer JL, eds. *Frontiers of Radiation Therapy and Oncology Vol. 25: The Role of High Energy Electrons in the Treatment of Cancer.* Basel: S. Karger AG, 1991:30–52, with permission.)

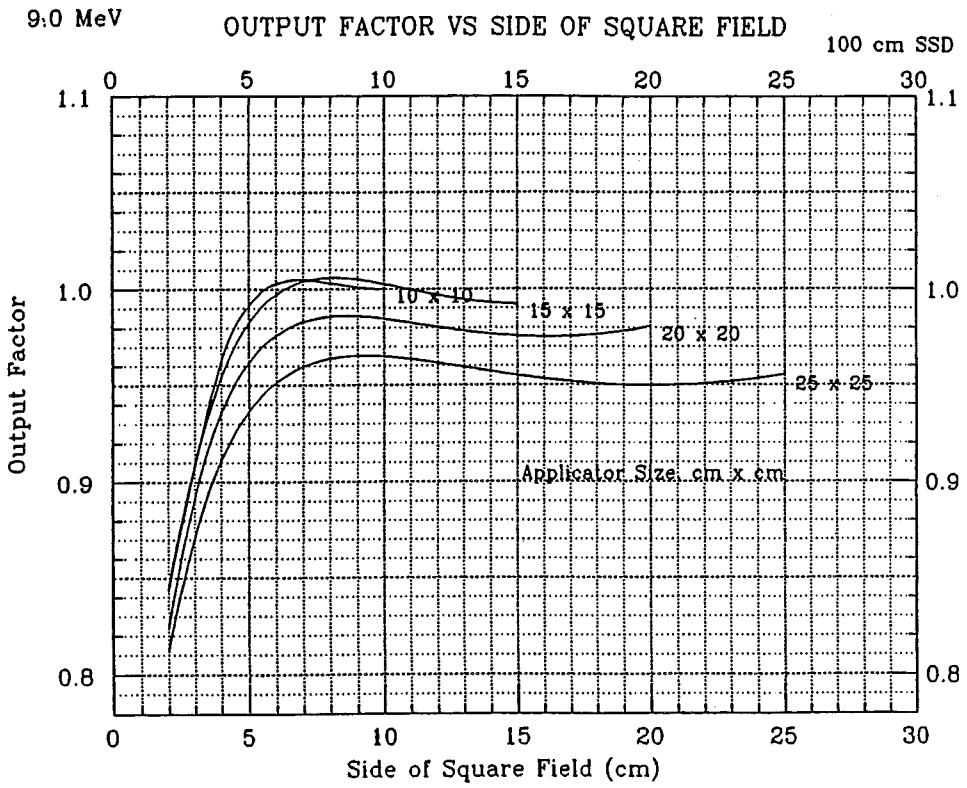

FIGURE 7.14. Field-size dependence of output (dose/monitor unit). Plot of output factor (cGy/MU) versus side of square field from 2 × 2 cm² to the open applicator for four applicators and for the 9-MeV beam of a Varian Clinac 2100C.

TREATMENT-PLANNING PRINCIPLES, TOOLS, AND METHODS

Electron therapy usually is restricted to a PTV that is within 6 cm of the patient's surface. Electrons may be used alone or in conjunction with photon beams. In the case of the former, the objective of the treatment planner is usually to select the appropriate beam direction, energy, and field size to provide as uniform a dose as possible to the PTV while delivering minimal dose to normal tissue and structures. To optimize dose homogeneity, the beam direction usually should be as close to normal incidence to the patient surface as practical. Once beam direction is specified, the selection of energy and field size specification follows. Figure 7.17 compares the isodose contours in water with the beam edges and R_{90}. Electrons are unique in that the uniform region of dose lies inside the 90% isodose contour. Dose in the patient outside the 90% isodose contour falls off rapidly. However, the patient anatomy can differ significantly from water so that effects resulting from patient heterogeneity make the resulting treatment plan unacceptable. Also, the PTV can be at a variable depth beneath the surface so that a single beam energy is inadequate. The treatment plan can be improved by utilization of special treatment aids such as skin or internal collimation, bolus, field abutment, or other special techniques.

Selection of Energy

The energy of the incident electron beam should be selected so that the distal surface of the 90% (of given dose) dose surface encompasses the PTV and that critical structures lie beyond the maximum penetration of the electrons or at an acceptable dose level. For planning purposes, a general rule is the following:

$$E_{p,0}(MeV) = 3.3 \cdot R_{90}(cm), \tag{7.6}$$

where $E_{p,0}$ is the most probable incident electron energy in MeV. The energy should be selected such that R_{90} exceeds the maximum depth of the PTV. This approximation is true in water for field sizes large enough to have side-scatter equilibrium on central axis. For small field sizes that do not have side-scatter equilibrium, R_{90} will be less, so a higher energy might be required. Also, heterogeneous tissue (e.g., bone or air) can affect the penetration requiring greater or lesser energy, respectively.

Similarly, for planning purposes, a general rule is the following:

$$E_{p,0}(MeV) = 2 \cdot R_p(cm), \tag{7.7}$$

where R_p is the practical range in centimeters of the electron beam (19). The treatment planner can select an energy such that R_p is less than the minimal depth of a critical structure. This approximation has no field-size limitation; however, as before, heterogeneous tissue (e.g., bone, lung, or air) can affect the penetration allowing greater or lesser energy.

As an example of how to use these general rules, consider irradiating the posterior cervical nodes of the neck with electrons to spare the spinal cord because its dose is already near tolerance. If the maximum depth of the nodes is 3 cm and the minimum depth of the spinal cord is 6 cm, then equations 7.6 and 7.7 indicate that the minimum energy to cover the PTV is 9.9 MeV and the maximum energy that protects the spinal cord is 12 MeV, respectively. Hence, beam energies in the range of 10 to 12 MeV should be acceptable. In all cases, the energy of the beam should be confirmed by performing a 3D dose

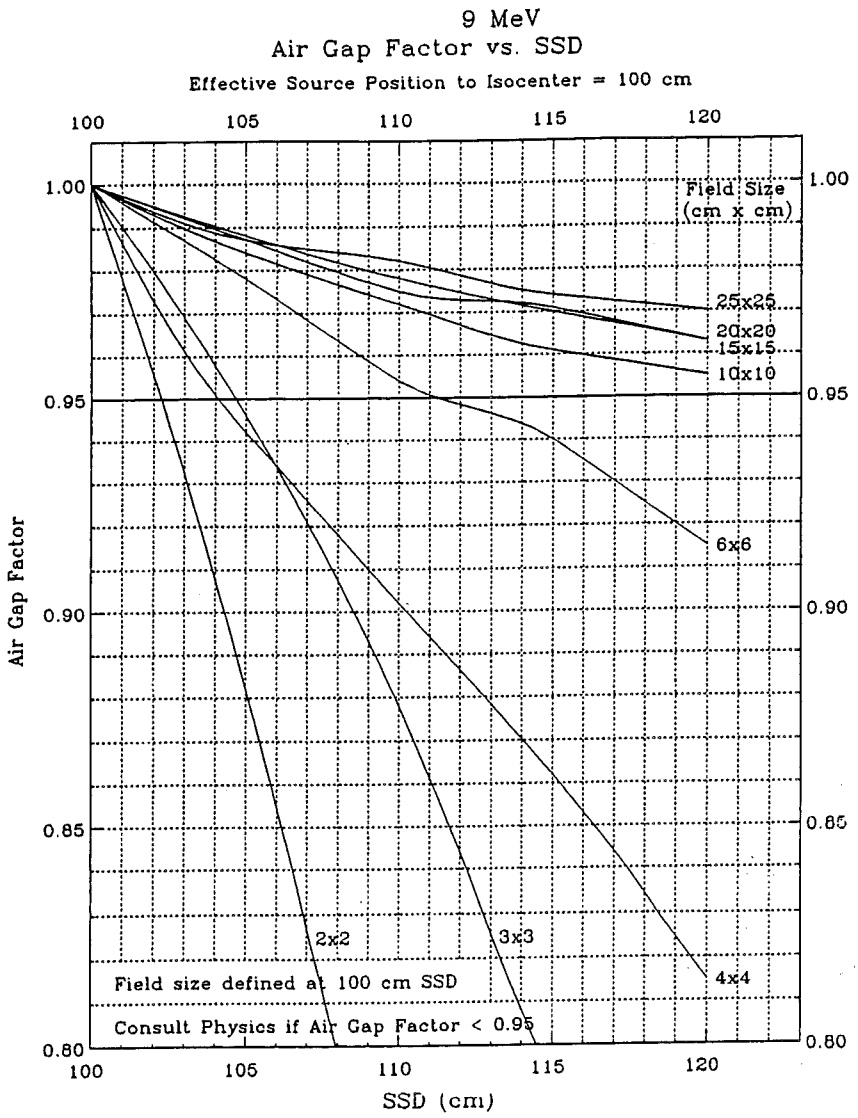

FIGURE 7.15. Dependence of air-gap factors on source-to-surface distance (SSD) and field size. Plot of f_{air} versus SSD for field sizes ranging from 2 × 2 to 25 × 25 cm^2 and for the 9-MeV beam (Varian Clinac 2100C).

calculation for the planned treatment using a CT representation of the patient.

Design of Electron Collimation

Electron collimation consists of multiple collimating components; however, the electron field shape usually is defined by an applicator's collimating insert and/or skin collimation. Custom electron collimators are constructed from lead or low-melting-point lead alloy (Lipowitz metal). The lead thickness in millimeters required to stop the primary electrons equals one-half the incident most probable energy of the electron beam in MeV (18,33). To account for small variations in thickness resulting from the lead-sheet manufacturing process, a 1-mm surplus can be added. That is,

$$t_{Pb}(mm) = 0.5 \cdot E_{p,0}(MeV) + 1. \qquad (7.8)$$

For example, an 18-MeV beam requires 10 mm of lead. Lipowitz metal has a density 20% less than that of lead; therefore, its thickness should be 20% greater. For example, an 18-MeV beam requires 12 mm of Lipowitz metal. Lipowitz metal collimating inserts usually are fabricated at a constant thickness—namely, that sufficient for the greatest energy on the treatment machine. For a machine whose maximum energy is 20 MeV, the Lipowitz metal thickness should be a minimum of 13 mm.

Skin collimation thickness is usually available in units of 1/16″ lead sheets and normally is taken to be the minimum thickness necessary to reduce the collimator's weight. The maximum possible dose beneath the skin collimation occurs at the skin surface with no air gap between the two (33,45). The transmitted dose, which is the result of bremsstrahlung photons from the incident beam and those generated by electrons stopping in the lead, is slightly greater than that with no lead present. It is recommended that a table of measured dose under the lead, as a function of lead thickness, is available for each beam energy (18). As the air gap between the lead and the patient increases, the transmitted dose to the patient decreases. These values can be measured at the time of beam commissioning. If not, and for cases where precise determination of dose beneath a block is critical, *in vivo* dosimetry (e.g., thermoluminescent dosimetry) should be used.

In designing the shape of the aperture of a collimating insert, due consideration is made for the penumbra. Typically, there

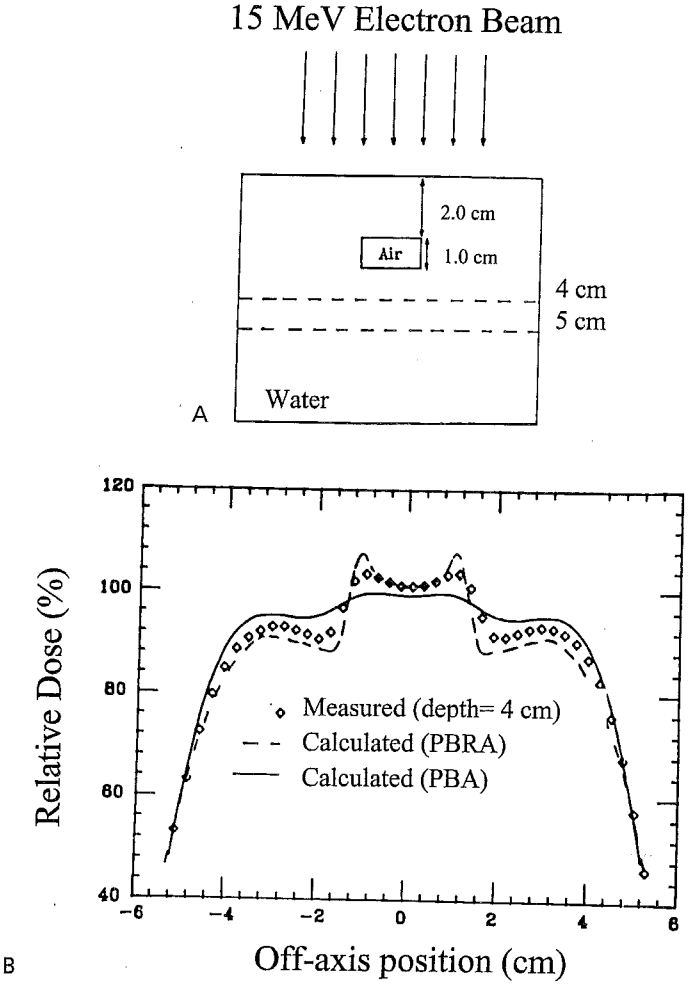

FIGURE 7.16. Evaluation of accuracy of dose algorithms below air cavity. **A:** Dose is measured distal to an internal air cavity. **B:** Measured dose profile at a depth of 4 cm is compared to that calculated by the pencil-beam algorithm and the pencil-beam redefinition algorithm. (From Shiu AS, Hogstrom KR. Pencil-beam redefinition algorithm for electron dose distributions. *Med Phys* 1991;18:7–18, with permission.)

is approximately a 1-cm margin between the projected edge of the collimator and outer boundary of target volume when both are projected to the isocenter. This margin varies with energy, depth, and air gap, and it only can be appreciated by utilization of isodose curves (Figs. 7.5 and 7.17). Again, the adequacy of the margin between the aperture and PTV should be confirmed by performing a 3D dose calculation for the planned treatment using a CT representation of the patient.

Skin Collimation

The closer the field-defining collimator is to the patient, the sharper the beam's penumbra; hence, skin collimation provides the sharpest possible penumbra. Because of the significant effort often required to fabricate skin collimation, its use is restricted to applications for which it has the greatest benefit, for example: (a) small-field treatments, (b) providing maximal protection to adjacent critical structures, (c) reducing penumbra beneath a bolus, (d) reducing penumbra when treating at an extended air gap, and (e) reducing penumbra in electron arc therapy. Proper

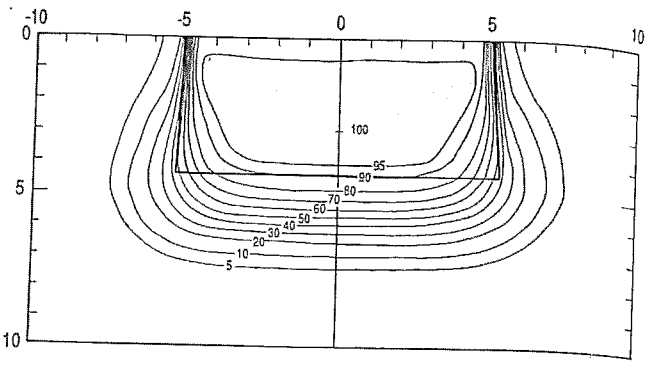

FIGURE 7.17. Plot of isodose curves for a 15-MeV, 10 × 10-cm² electron beam in water (source-to-surface distance, or SSD = 100 cm). Note the shape of the 90% isodose contour with respect to the shaded area, which is framed by the diverging field edges and the R_{90} depth.

use of skin collimation requires that it be in contact with the skin surface and that it extend sufficiently inwardly and outwardly to intercept the penumbra from upstream collimation (18,19,20).

The utility of skin collimation for small-field treatments is illustrated in Fig. 7.18. A 6-MeV, 3 × 3-cm² field with a 10-cm air gap (collimator to surface) is essentially all penumbra, resulting

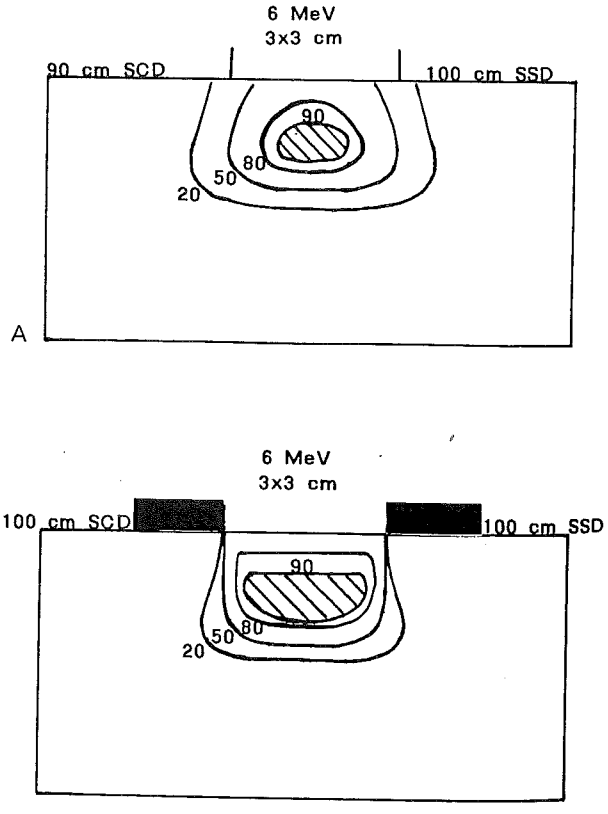

FIGURE 7.18. Impact of skin collimation for small electron fields. Isodose plots are compared for results of a computer simulation of a 6-MeV electron beam in water for **(A)** a 3 × 3-cm² field formed by an applicator insert 10 cm above the patient and **(B)** a 3 × 3-cm² field formed by collimation at the surface with a 6 × 6-cm² applicator insert 10 cm above the patient. (From Hogstrom, KR. Clinical electron beam dosimetry: basic dosimetry data. In: Purdy JA, ed. *Advances in Radiation Oncology Physics: Dosimetry, Treatment Planning, and Brachytherapy.* Woodbury: American Institute of Physics, Inc.,1991:390–429, with permission.)

in an unsatisfactory dose distribution. However, by opening the collimator to 6 × 6 cm^2 and then forming the 3× 3-cm^2 field using skin collimation, the dose distribution becomes clinically satisfactory. This application is used for treatment of the eyelid, nose, and other small target volumes.

In the presence of skin collimation, the depth dose is approximated by that for the field size on the skin surface (i.e., that defined by the skin collimator). In contrast, the dose output is approximated by that for the field size incident on the skin collimation (i.e., that defined by the applicator cutout). For the example in Fig. 7.18, the depth dose is taken to be that of the 3 × 3-cm^2 field; the dose output is taken to be that of the 6 × 6-cm^2 field. This simple approximation slightly overestimates dose output, if the depths of maximum dose for the two field sizes differ. In such a case, the output of the larger field is multiplied by the depth-dose factor of the larger field at the depth of maximum dose of the smaller field (28).

Figure 7.19 illustrates the use of skin collimation for postoperative treatment of the nose when uniform thickness bolus is placed off the surface. Rules for skin collimation when an air gap between the bolus and patient exists are given by Hogstrom (19).

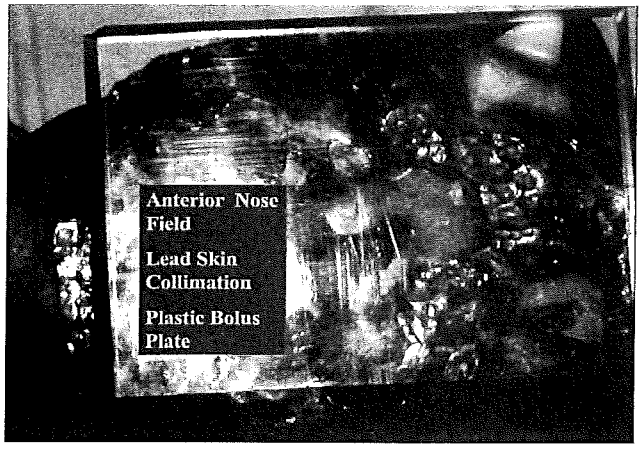

FIGURE 7.19. Skin collimation under bolus. Skin collimation is used to restore penumbra under a bolus placed off the patient surface in postsurgical electron therapy of the nose.

Bolus

Bolus is an essential tool for the delivery of optimal electron radiation therapy. Electron bolus is defined as water or near-water-equivalent material that normally is placed either in direct contact with the patient's skin surface, close to the patient's skin surface, or inside a body cavity. This material is designed to provide extra scattering or energy degradation of the electron beam. Its purpose usually is to shape the dose distribution to conform to the target volume or to provide a more uniform dose inside the target volume (18,19). More specifically, electron bolus has three primary applications:

1. To increase dose to the patient's external surface
2. To serve as a missing tissue compensator for surface irregularities and internal air cavities
3. To shape the coverage of the treatment volume to conform as closely as possible to the target volume while avoiding critical structures

In the second application, bolus is being used to either eliminate or decrease the adverse effects of patient heterogeneities on the dose distribution, which can result in a geographic miss at depth, dose nonuniformity within the target volume, and excessive dose to distal critical structures (18,19).

Because dose typically is prescribed to 90% to 100% of the given dose, it is often desirable to increase surface dose to 90% or higher when treating with low-energy electrons. To accomplish this, a higher energy beam is selected and a uniformly thick bolus is placed on or near the skin surface. The surface dose of the higher energy electron beam is greater, and the bolus places the skin at a deeper depth, further increasing the surface dose. The energy-bolus thickness combination is selected to place R_{90} at the prescription depth while increasing the surface dose (D_s) to near 90%. To assist in usage of this technique, a table that allows selection of the optimal energy-bolus thickness combination is recommended. Table 7.1 illustrates a sample table for

TABLE 7.1. VALUES OF SURFACE DOSE AND THERAPEUTIC DEPTH FOR VARIOUS ENERGY-BOLUS COMBINATIONS

Superflab Thickness (cm)	0.0	0.3	0.5	1.0	1.5	2.0
Energy: 6 Mev						
D_s (%)	72	79	83	93	100	–
R_{90} (cm)	2.0	1.7	1.5	1.0	0.5	–
Energy: 9 Mev						
D_s (%)	78	83	85	89	95	99
R_{90} (cm)	3.0	2.7	2.5	2.0	1.5	1.0
Energy: 12 Mev						
D_s (%)	83	88	89	91	94	96
R_{90} (cm)	4.0	3.7	3.5	3.0	2.5	2.0
Energy: 16 Mev						
D_s (%)	87	92	93	96	97	98
R_{90} (cm)	5.0	4.7	4.5	4.0	3.5	3.0
Energy: 20 Mev						
D_s (%)	91	96	97	98	99	100
R_{90} (cm)	6.1	5.8	5.6	5.1	4.6	4.1

the five electron beam energies of a typical radiation therapy machine.

Two bolus methods are used for this function. One places flexible sheet material (e.g., Superflab) directly on the skin surface. This material is approximately water equivalent and comes in thickness increments of 0.3 cm to 4 cm. It is particularly useful for chest-wall irradiation, both for fixed-beam and arced-beam therapies. In some treatments, the bolus is used for only a portion of the field, in which case care must be taken to ensure the edge of the bolus is tapered to reduce the magnitude of the hot or cold spot created by the surface irregularity (c.f. Fig. 7.7) (18,19).

For highly irregular or sensitive skin surfaces, which often are encountered in head and neck or postsurgical irradiations, it is advantageous to have a rigid bolus sheet (often referred to as a "scatter plate" because it not only degrades the energy of the electron beam but also scatters the beam) close to but not necessarily in direct contact with the patient (19). For such cases standard thicknesses of polymethylmethacrylate (PMMA) (1/8″ to 1/4″) are placed perpendicular to the beam, as illustrated in Fig. 7.19. To restore a sharp penumbra, skin collimation usually is recommended with use of the scatter-plate bolus method. Rules for using skin collimation with the bolus have been discussed by Hogstrom and colleagues (19). It is important that the bolus be in contact or close to the patient because too large of an air gap can create an exceedingly large penumbra. This is demonstrated in Fig. 7.20, where a 5-cm air gap results in a 50% decrease in the given dose because of the bolus scattering electrons away from the field.

Bolus is considered part of the beam; however, it also can be considered part of the patient, effectively shortening the SSD. For uniform bolus thickness (t), it is recommended to adjust the dose output for inverse square (28). That is,

$$O_{bolus} = O \cdot \left[\frac{SSD + t + R_{100}}{SSD + R_{100}}\right]^2. \qquad (7.9)$$

A variety of methods exist for using bolus to remove surface irregularities, which result in volumes of overdose and underdose resulting from scatter inequilibrium if ignored (15,19). One method involves fabrication of a beeswax bolus onto a positive cast of the patient, as used for treatment of carcinoma of the nose (Fig. 7.21). In this case, the bolus is used to surround the protrusion of the nose with scatter material. In other applications, air cavities, such as the ear canal (Fig. 7.8) (50), or surgical defects are filled with a saline solution, water-filled bags, or wax or Superflab customized to fit the defect. In each of these applications, the philosophy is to make the patient as much like a flat-surfaced water phantom as possible.

A more sophisticated use of bolus is to design custom bolus for the purpose of electron conformal therapy. In this application, the bolus usually is designed to conform the 90% isodose line to the PTV while minimizing dose to nearby critical structures and maintaining dose uniformity as much as possible within the 90% dose contour. Proper design of custom bolus requires use of a 3D treatment-planning system (61) that utilizes bolus design operators (39) and a 3D PBA (62). Perkins and colleagues (53) have demonstrated the use of custom bolus for chest-wall irradiation in the cases of highly distorted anatomy and of a chest wall recurrence (Fig. 7.22), and Kudchadker and colleagues (36) have demonstrated its use in head and neck treatment. Low and

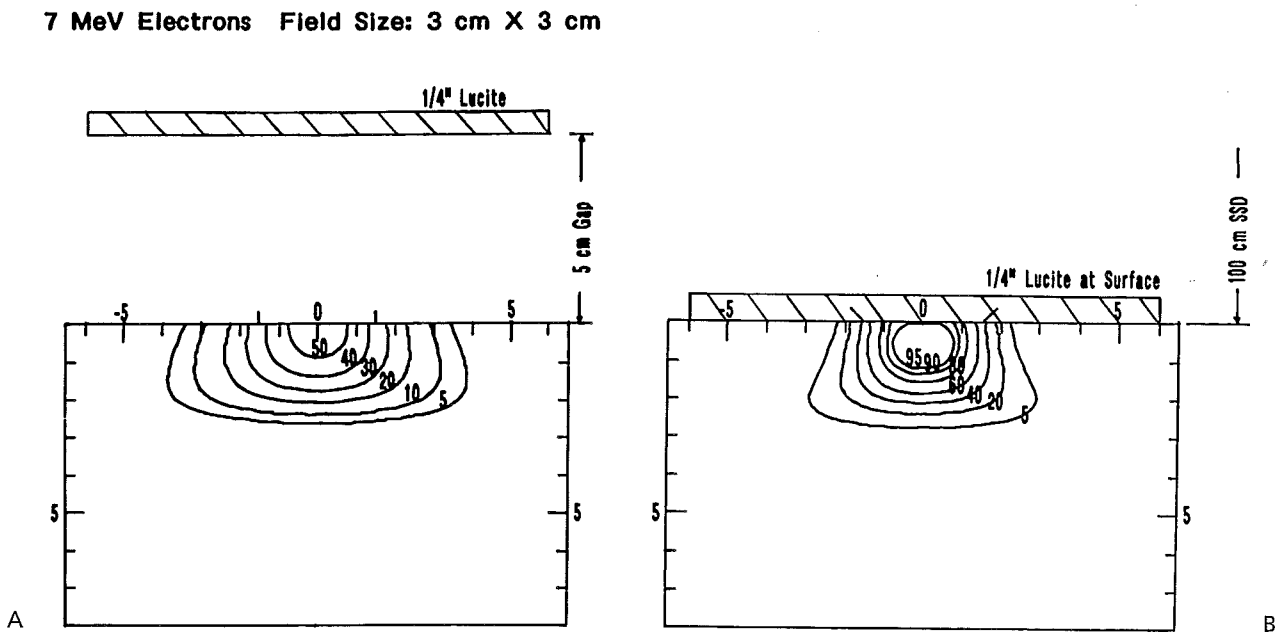

FIGURE 7.20. Proper location of slab bolus. Constant thickness (slab) bolus is used to increase surface dose and to fine tune electron-beam penetration (Table 7.1). Its location is important for irradiation by a small field (3 × 3 cm^2) and low energy (7 MeV) electron beam. **A:** If a 1/4″ PMMA plate is located 5 cm above patient, electrons are scattered away from the field resulting in needless broadening of the penumbra and a decrease in given dose of approximately 50% (given dose without the bolus is 100%). **B:** Placing the 1/4″ PMMA plate on the surface preserves both the given dose and beam penumbra.

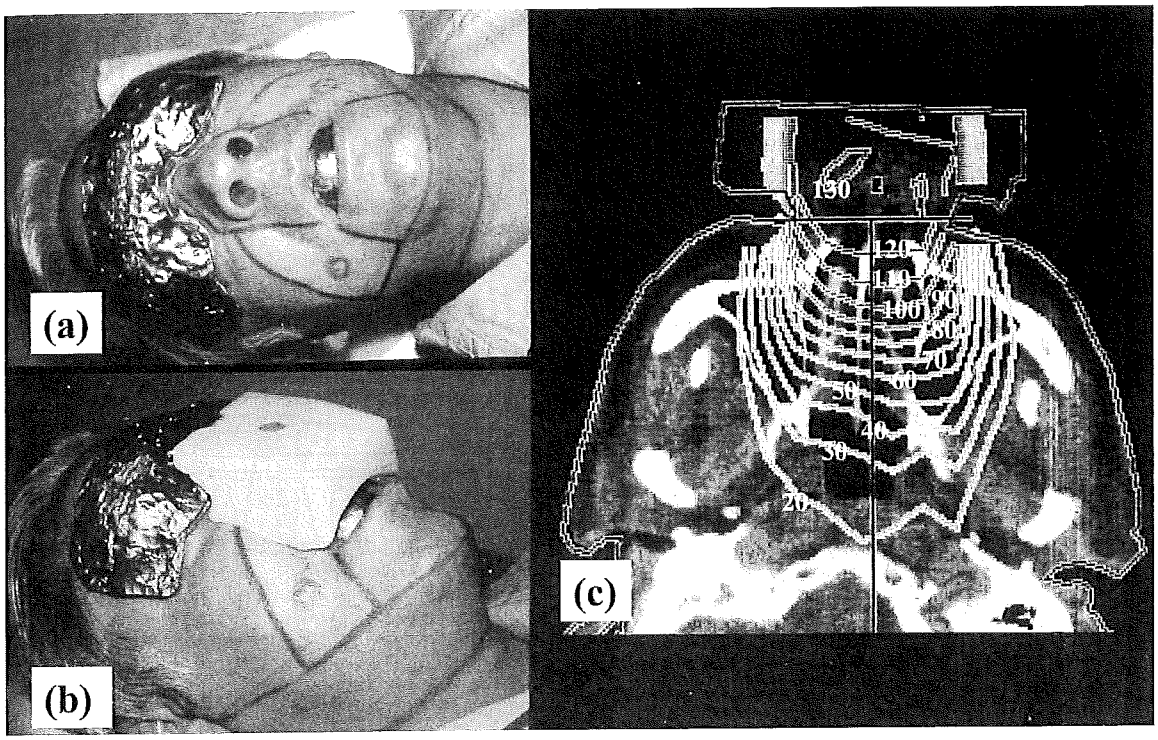

FIGURE 7.21. Utility of bolus to remove dose inhomogeneity caused by surface irregularity of nose. **A:** Bolus in nasal air passages prevents cold spots in the septum (Fig. 7.10). (Also, note the skin collimation used to restore penumbra under nose bolus and the intraoral stent used to protect the tongue.) **B:** Wax bolus surrounding the nose eliminates irregular patient surface. **C:** Isodose curves superimposed on a transverse computed tomography scan illustrate how the bolus makes the patient more like a water phantom, resulting in a homogeneous dose distribution characteristic of that in a water phantom. The patient dose is delivered 12-MeV electrons: ^{60}Co photons = 4:1. (Note that the surface dose is lower than that shown because the treatment-planning system calculated the photon dose assuming the bolus was in place during its delivery, which is not the case.) (From Hogstrom KR. Treatment planning in electron beam therapy. In: Vaeth JM, Meyer JL, eds. *Frontiers of Radiation Therapy and Oncology Vol. 25: The Role of High Energy Electrons in the Treatment of Cancer.* Basel: S. Karger AG, 1991:30–52, with permission.)

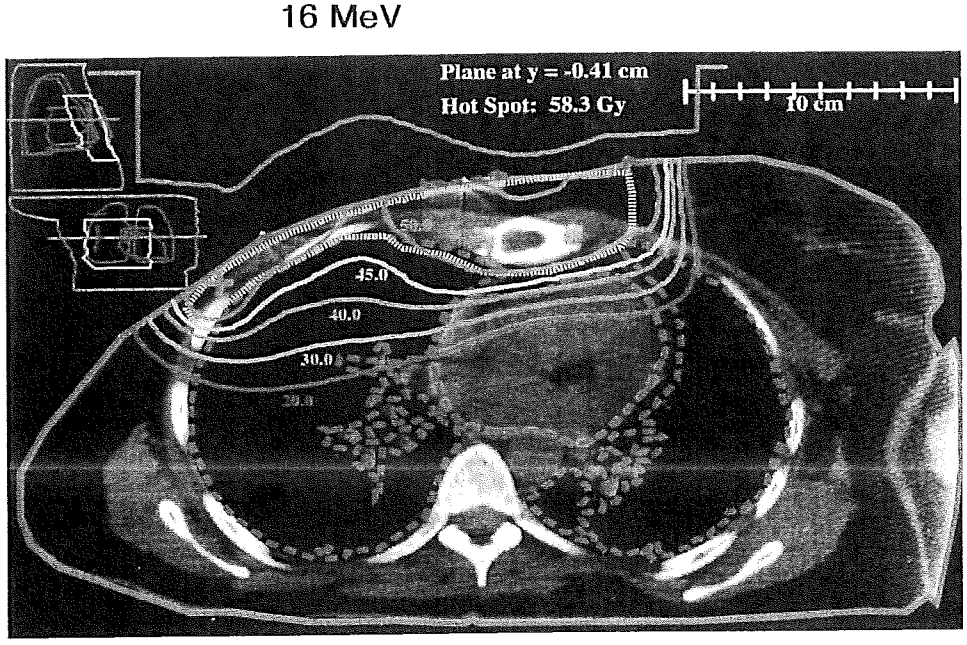

FIGURE 7.22. Conformal electron therapy using variable thickness bolus. Bolus is used to shape the 90% isodose surface (45 Gy) to the distal surface of the chest wall in treating a chest wall occurrence, optimally sparing lung. (From Perkins GH, McNeese MD, Antolak JA, et al. A custom three-dimensional electron bolus technique for optimization of postmastectomy irradiation. *Int J Radiat Oncol Biol Phys* 2001;51:1142–1151, with permission.)

associates (40) have shown its utilization for sparing spinal cord, lung, and kidney in treatment of the paraspinal muscles.

It is recommended that the intent of bolus be verified by measurement or calculation. Bolus used to increase skin dose can be verified by performing *in vivo* dosimetry measurements (e.g., using thermoluminiscent dosimetry). Complex bolus shapes, as used to remove surface irregularities or for electron conformal therapy, can be verified by CT scanning the patient with the bolus in place (40,53). The dose distribution then can be recalculated using the electron dose algorithm in a treatment-planning system.

Internal Collimation

Internal collimation stops electrons that enter the body before they reach critical structures and deposit any significant dose. Examples of clinical utilization of internal collimation are intraoral blocks protecting salivary glands during head and neck treatments (64); eye blocks protecting the lens in irradiation of the eyelid (58), orbit, or retina; and sheets of lead used to protect internal structures during intraoperative therapy.

There are two concepts important to remember in the use of internal collimation. First, the collimator must be sufficiently thick to stop the energy of the electrons in the beam at depth. Electron-beam energy is reduced by 2 MeV per cm in unit density tissue; hence, the energy of a 12-MeV beam at a depth of 2 cm is 8 MeV. The thickness of lead required to stop 8-MeV electrons is 4 mm (8 MeV · 0.5 mm/MeV).

One application where ensuring that collimation is sufficiently thick that has been sometimes overlooked is the use of internal eyeshields. Shiu and associates (58) showed that *x-ray* eyeshields constructed of plastic-coated lead and designed to shield the eyes from kilovoltage x-rays did not stop 6-MeV electrons, resulting in penetration of approximately 50% of the given dose. However, *electron* eyeshields constructed of enamel-coated tungsten can stop electrons with energies as great as 9 MeV (Fig. 7.23). By using higher density tungsten ($\rho = 19.3$) instead of lead ($\rho = 11.5$), the eyeshields remain sufficiently thin to fit under the eyelid. If only x-ray eyeshields are available, bolus should be placed on top of the eye and eyeshield to ensure that the electron energy is reduced sufficiently so that electrons do not penetrate the eyeshield.

Second, electrons backscattered from lead at a lead-tissue interface increase dose, the increase ranging from approximately 20% at 20 MeV to 60% at 4 MeV, where the energy is the average energy of electrons incident on the lead (33,35). Inserting two half-value layers of bolus between the lead and the tissue usually reduces the dose to upstream tissue to a clinically acceptable value. The thickness of one half-value layer ranges from approximately 1 cm at 10 MeV to 0.5 cm at 3 MeV (33,38). Intraoral lead stents are coated with acrylic routinely (64), and a material such as dental wax can be applied easily to lead sheets placed between the mucosa and gums. Eyeshields, however, only have clearance for 1 to 2 mm of coating; hence, backscatter dose to the eyelids is important in treatment management (58).

Field Abutment

The purpose of field abutment usually is to enlarge the radiation field or to change the beam energy or modality. In either case, beam uniformity requires that three criteria be met.

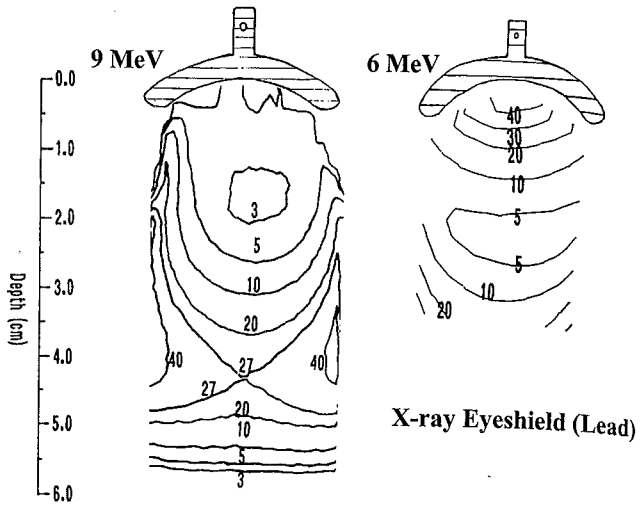

FIGURE 7.23. Electron eyeshields. The dose distribution under tungsten electron eyeshields demonstrates its ability to stop 9-MeV electrons. The dose distribution under a lead x-ray eyeshield shows its inability to stop 6-MeV electrons. (From Shiu AS, Tung SS, Gastorf RJ, et al. Dosimetric evaluation of lead and tungsten eye shields in electron beam treatment. *Int J Radiat Oncol Biol Phys* 1996;35:599–604, with permission.)

First, the beams must abut along the entire border (18,19,30,33). If the edges of the two beams coincide exactly (Fig. 7.24A), then the two beams will be equivalent to a single beam and optimal uniformity will be achieved. This type of beam arrangement frequently is used for electron-beam irradiation of the spine as part of craniospinal irradiation. If the central axes of the two beams are parallel (Fig. 7.24B), then the diverging beam edges will overlap, creating a cold spot upstream and a hot spot downstream of the region of intersection. This is least significant for narrow fields, as encountered in irradiation of the cervical nodes of the neck or abutting the internal mammary and medial chest-wall fields. If the central axes are converging (Fig. 7.24C), then there is an even greater amount of overlap. This is the case for abutting lateral and medial chest-wall fields. In such cases, feathering the beam edge ± 1 cm can reduce the dose heterogeneity. This is illustrated in Fig. 7.25 for a standard postmastectomy chest-wall irradiation using electrons.

The second criteria is that the beam penumbra must be matched. This is the case for the two spinal fields referred to earlier, but it is not the case in general, particularly in abutting electron to photon fields. In such cases, either one or both of the field edges must be feathered. Third, it is best that the penumbra be somewhat broad. This reduces the impact of misalignment on the uniformity of dose in the abutted region.

Circular Anatomy

There are two different techniques for treating cylindric anatomy, each resulting in differing dose distributions. Each of the techniques irradiates from multiple beam directions encircling the anatomy either using multiple fixed-beams or arc therapy. First, consider the case in which the electron beams are broad compared to the anatomy, in which case many electrons graze the anatomy,

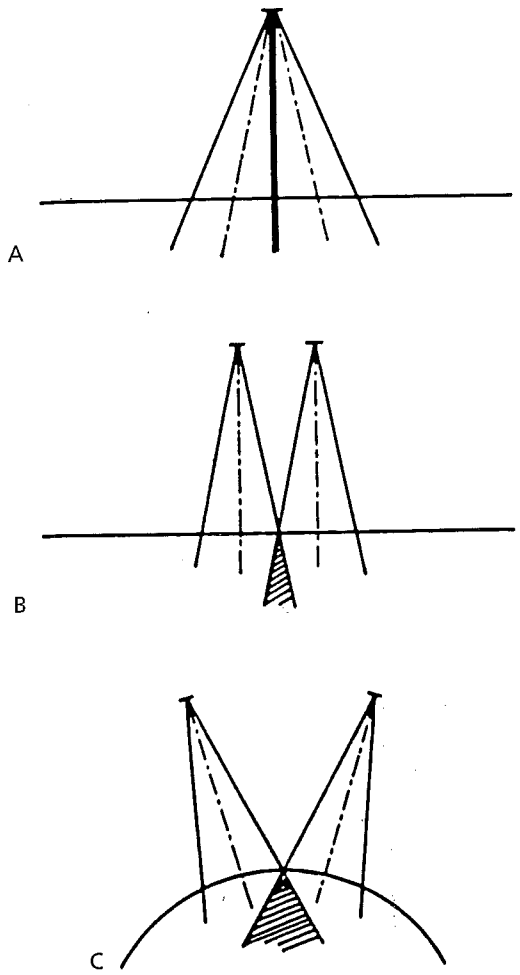

FIGURE 7.24. Comparison of abutment geometries. **A:** Common edge is created by having diverging central axes. **B:** Parallel central axes result in overlapping edges. **C:** Converging central axes result in the greatest overlap. (From ICRU Report 35. *Radiation dosimetry: Electron beams with energies between 1 and 50 MeV.* Bethesda: International Commission on Radiation Units and Measurement, 1984, with permission.)

resulting in increased surface dose and less beam penetration. This is the case for total limb irradiation and total skin irradiation, both of which use 6 to 8 beam directions. Figure 7.26A shows the depth dose resulting from an eight-field technique using 6-MeV electron beams to irradiate a 20-cm diameter phantom.

In contrast, consider the case where the beam is narrow, representing the geometry most typical of electron arc therapy of the chest wall. The resulting depth dose for a 7-MeV beam rotating around a 20-cm diameter cylinder is seen in Fig. 7.26B. The narrow beam results in the average direction of the electrons being perpendicular to the surface (i.e., focused toward isocenter). This results in the electrons being closer together as depth increases, which results in an increased fluence and dose. This increase results in a depth-dose curve with a more significant build-up of depth dose and sharper fall-off.

Mixed-Beam Therapy

Electron beams frequently are mixed with photon beams to create an appropriate treatment. The mixed beams can irradiate a common volume of tissue, or they can be abutted. In the former case, an electron field may be added to a primarily photon-beam treatment or a photon field may be added to a primarily electron-beam treatment. For example, electron boosts are used to deliver localized dose to the surgical site following photon breast irradiation, to treat the postcervical nodes once spinal cord tolerance is reached, and to reduce spinal cord dose (e.g., in lymphoma treatment) (47). In some head and neck treatments, the photon beam is a surrogate to the electron beam, being used to reduce skin dose and to increase dose penetration while still sparing the contralateral salivary gland (14,64). With the future availability of intensity-modulated x-ray and electron therapy, the effectiveness of mixed-beam therapy can be expected to increase in breast and head and neck radiation therapy.

Abutted mixed beams are used when separate portions of the anatomy can benefit from the two individually. The most common application of this process is the utilization of electron fields for irradiation of the internal mammary chain, supraclavicular, or axillary lymph nodes as part of breast or chest-wall irradiation (64). This technique is also used for irradiating the total scalp or for craniospinal irradiation, which are described later.

SPECIALIZED ELECTRON TECHNIQUES

Although electron-beam therapy is used less frequently than is photon beam therapy, it remains an essential modality. To fully use electron-beam therapy, there must be access to comprehensive electron treatment and treatment-planning techniques. This includes specialized electron techniques, which, in the present context, are defined as those that are seldom required and that use a complex treatment geometry, special treatment delivery hardware, or special treatment-planning software. It is not recommended that all radiation therapy facilities offer all techniques, but radiation oncologists should be aware of these techniques and should be able to refer patients to a regional center for those that are impractical in smaller settings. This recommendation is based on the significant time, resources, and costs of implementing, maintaining, and providing some of the more complex special electron procedures. The American College of Medical Physics has reviewed the effort and cost associated with several special procedures, which include electron arc therapy, intraoperative electron therapy, and total-skin electron irradiation (22).

Four types of special techniques are discussed here. First, the treatment of internal tissues is exemplified by intraoperative radiation therapy and intracavitary radiation therapy. Second, the utilization of abutted electron and photon fields is exemplified by craniospinal and total-scalp treatment techniques. Third, the treatment of superficial tissues for a cylindric geometry is exemplified by the total-limb and total-skin treatment techniques. Fourth, an alternative to fixed-beam therapy of the chest wall is exemplified by arc therapy.

Intracavitary Irradiation

Cones of appropriate design can be used for intracavitary electron irradiation, which delivers an improved dose distribution over that traditionally delivered using orthovoltage x-rays. Intracavitary irradiation most frequently is used to boost

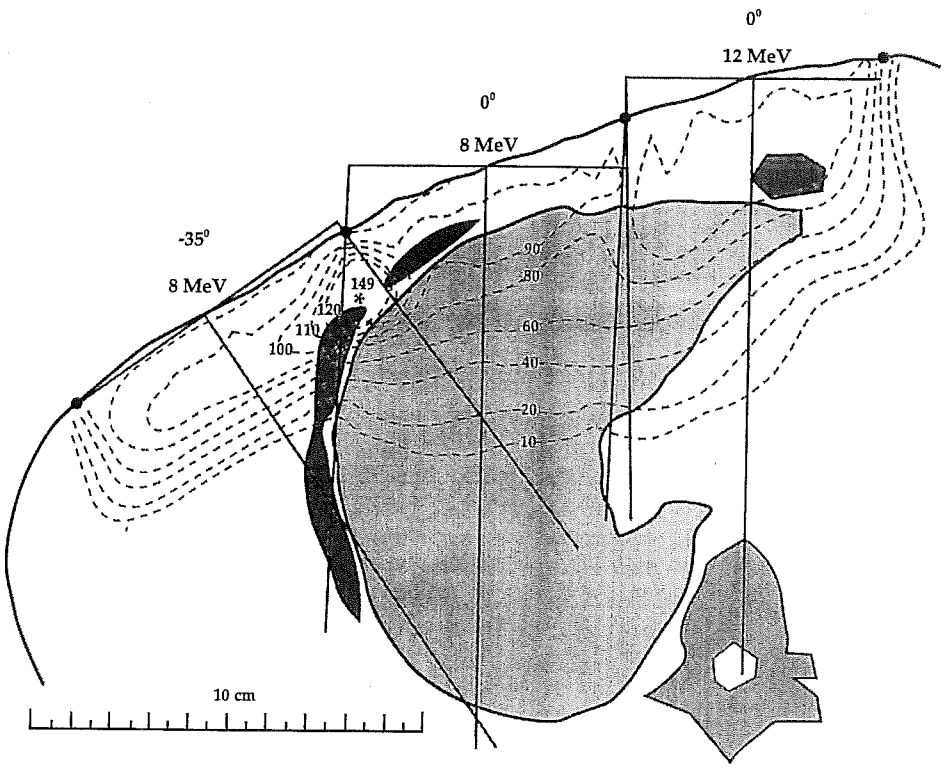

FIGURE 7.25. Clinical example of abutting electron fields in chest wall treatment. Dose homogeneity is acceptable at the border of internal mammary chain (IMC) and medial chest-wall fields because central axes are parallel and field widths are small. Dose homogeneity is unacceptable at the border of medial and lateral chest-wall fields because central axes are converging (Fig. 7.11B). Dose homogeneity is improved at border of medial and lateral chest-wall fields by delivering equal doses with the match line being moved 1 cm twice during treatment.

the primary site while sparing nearby normal tissues. Intracavitary irradiation has been a choice for intraoral, transvaginal, and intraoperative treatments. Wang (67) showed the benefit of intraoral cones for boosting the oral lesions of the floor of the mouth, soft palate, tongue, and retromolar trigone while sparing mandible, teeth, gum, and salivary glands. McGinnis and colleagues (43) reported using a transvaginal cone to boost carcinoma of the cervix with electrons, reducing bulk tumor to subsequently allow intracavitary brachytherapy. Intraoperative radiation therapy can be used in many sites (66); however, it is used primarily for abdominal sites. Merrick and associates (44) reviewed the experience of the United States in use of intraoperative radiotherapy for treatment of pancreatic, biliary, and gastric carcinomas.

The criteria for intracavitary electron irradiation are similar, regardless of site. A treatment cone is necessary in order that healthy tissue can be restrained from intercepting electrons irradiating the tumor. The cone wall must be sufficiently thick to stop electrons from escaping to outside tissue while being thin enough not to interfere with tumor access. Guidelines for accomplishing this for intraoperative cones have been discussed by Hogstrom and colleagues (20). Another issue is how to ensure accurate alignment while maintaining patient safety with a cone. Appropriate cone positioning requires having a method for looking down the cone to view the tumor. Proper alignment of the cone after inserting it into the patient requires methods for docking it to the machine. For soft docking, the cone is not physically attached to the machine (Fig. 7.27) (20). For hard docking, the cone is physically attached to the machine, and there are methods for its breaking away under stress (6,43). Many of the intraoral and transvaginal cones are x-ray cones converted for use with electrons; however, intraoperative cones are larger and typically designed for that specific purpose.

Treatment planning for intracavitary cones typically is done manually because it is not possible to CT scan the patient in the treatment position or under operating-room conditions. The electron energy and cone size are selected to match measured isodose distributions to the dimensions of the clinical target volume. Examples of dose distributions for intraoperative cones are shown in Fig. 7.28. These examples show two characteristics of such cones. First, for the larger diameter cones, scatter off the wall of the cone can lead to hot spots near the cone's periphery. Second, ends of the cones often are beveled to make it easy to establish contact when the anatomic plane is not perpendicular to the direction of approach (i.e., the central axis of the beam). Note how the depth of the 90% isodose contour beneath the surface decreases from 3.6 cm at 0° incidence to 3.0 cm at 30° incidence, as a result of the effects described earlier.

Craniospinal Irradiation

Craniospinal irradiation is important for management of brain tumors that seed along the pathways of the cerebrospinal fluid (e.g., medulloblastoma, malignant ependymoma, germinoma, and infratentorial glioblastoma) (41). Utilization of a high-energy electron beam in lieu of photons to irradiate the spinal cord can reduce dose to the upper aerodigestive and lower gastrointestinal tracts, lymph nodes, and the vertebral bodies. This should result in reduced probability to acute complications and late effects (41,42). Challenges to this technique are (a) proper selection of energy to account for effect of bone; (b) abutment scheme in the neck to achieve uniform dose at the abutment of the posterior

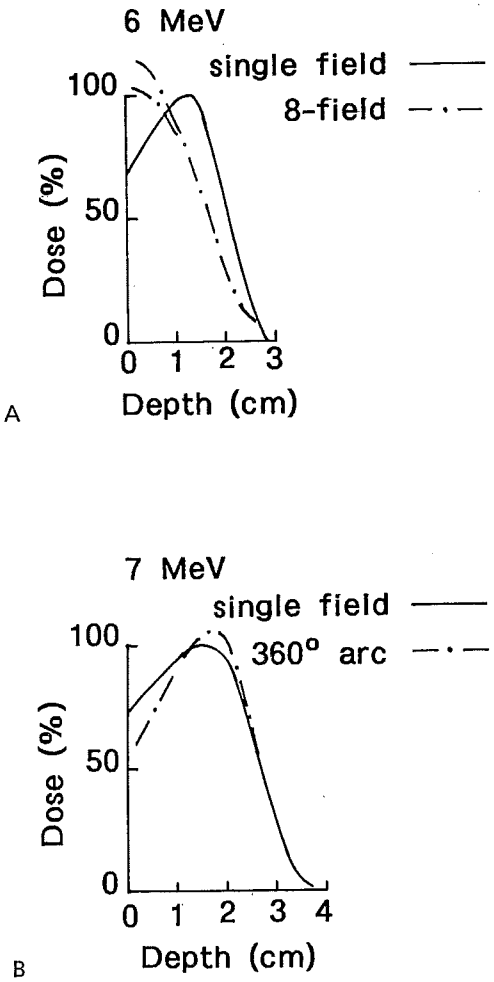

FIGURE 7.26. Treating circular anatomy with multiple beams spaced over 360°. Depth dose along a radial axis depends on the field width. **A:** Depth dose for a broad, 6-MeV beam, resulting from an 8-field technique around a 20-cm diameter water cylinder, is governed by grazing radiation, typical of total-skin and total-limb irradiation. **B:** Depth dose for a narrow, 7-MeV beam, resulting from rotating around a 20-cm diameter water cylinder, is governed by focusing of the radiation toward isocenter, typical of arc electron therapy.

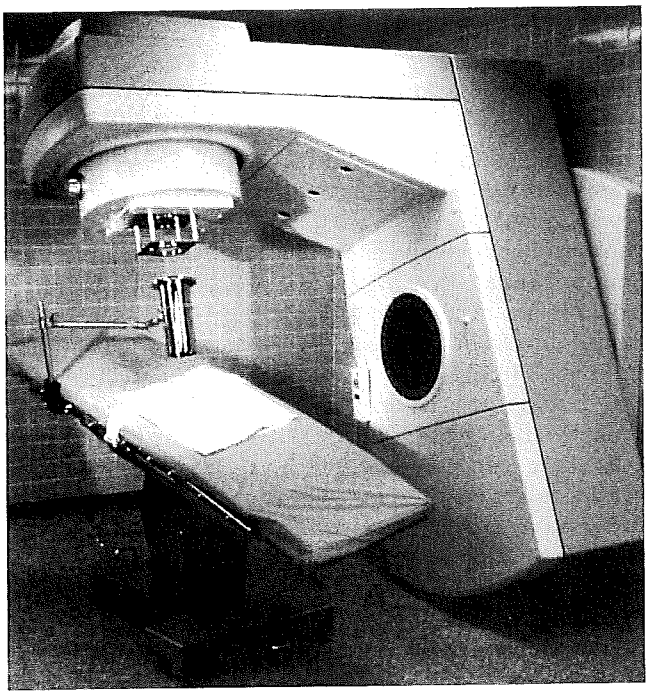

FIGURE 7.27. Intraoperative electron radiation therapy accelerator. View of dedicated Siemens intraoperative radiation therapy unit in operating room. Note the separation between the treatment cone and the radiation therapy treatment head. A laser alignment system provides soft docking between treatment head and the cone (20).

electron field of the spine with the parallel opposed, lateral photon fields irradiating the brain; and (c) abutment scheme for the two electron fields usually used to treat the spine. Two similar techniques for craniospinal techniques are reported by Maor and colleagues (41,42) at M.D. Anderson Cancer Center and by Dewit and associates (10) at University Hospital in Leuven. The former is described here.

The fundamental geometry of the technique is illustrated in Fig. 7.29. The electron field usually is placed at 110 to 115 SSD, which increases both its usable length and the width of its penumbra, the latter making it more suitable for abutment. The minimum electron energy is selected so that the 90% isodose surface encompasses the spinal cord. The R_{90} of the electron beam in water should exceed the maximum depth of the spinal cord by 7 mm—4 mm to account for increased energy loss in the bone and 3 mm as a margin for error (41). If the depth of the spinal cord varies significantly, then bolus along the spinal field is used to conform the 90% isodose surface to the anterior border of the spinal cord (Fig. 7.30). Today, the resulting treatment plan can be confirmed using a 3D treatment-planning system to calculate dose.

The length of the spinal cord often exceeds the maximum electron field length along the major axis of an applicator (e.g., for a 25 × 25-cm^2 applicator, 27.5 cm at 110-cm SSD). In such cases, the field length can be increased by using a diagonal cutout (e.g., for a 25 × 25-cm^2 applicator, approximately 32 cm at 110-cm SSD), by abutting two electron fields, or both. Maor and colleagues (41) recommend abutting using the common-edge technique. This technique for abutting two electron fields of 27.5-cm length or less using the 25 × 25-cm^2 applicator is shown in Fig. 7.30. It requires rotating the table to 90° and rotating the gantry ($\theta/2$) from true vertical to exactly match the beam edges. This ensures a uniform dose throughout the abutment region; however, care must be taken to accurately match the edges of the abutted radiation fields. For example, current Varian accelerators do not have light field-radiation field agreement because of their light source being approximately 11 cm from the virtual electron radiation source (60). Thus, when abutting 27.5-cm wide fields at 110-cm SSD, it is necessary to leave a 5-mm gap in the light fields to match the 50% OARs of the two fields and to avoid overdosing the cord.

The other challenge is to achieve uniform dose in the abutment region of the electron and photon fields. This is achieved by first rotating the x-ray collimators (θ) to align the inferior edges of the parallel-opposed x-ray fields with the superior, diverging edge of the electron field. It is also beneficial to place the isocenter as close

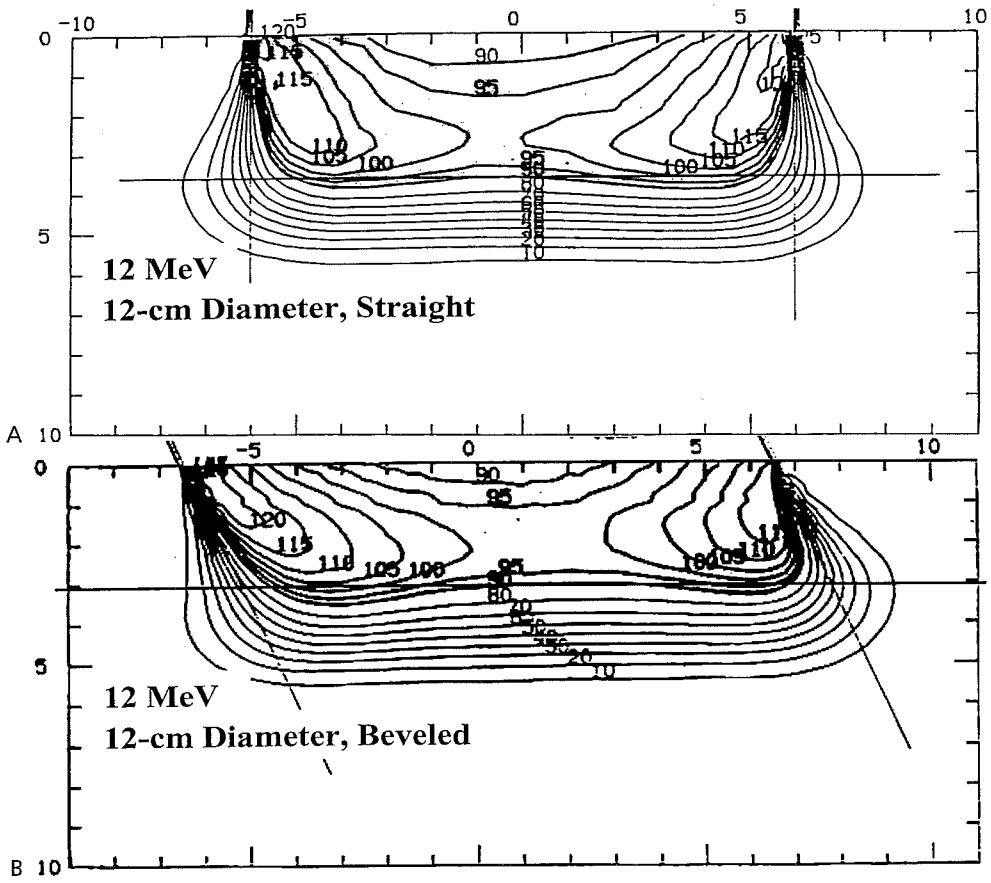

FIGURE 7.28. Isodose plots illustrating typical intraoperative dose distributions at 12 MeV. **A:** 12-cm diameter cone, normal incidence and **(B)** 30° beveled, 12-cm diameter cone. Note the decreased depth of the 90% dose beneath the surface for the beam 30° from normal incidence relative to that for normal incidence. (From Nyerick CE, Ochran TG, Boyer AL, et al. Dosimetry characteristics of metallic cones for intraoperative radiation therapy. *Int J Radiat Oncol Biol Phys* 1991;21:501–510, with permission.)

as possible to the abutment region because this eliminates effects from beam divergence in the cephalocaudal direction. Because the photon penumbra is significantly sharper than that of the electron beam, its edge is feathered (typically ± 9 mm) to produce a penumbral width similar to that of the electron beam. To achieve the most uniform fraction dose, one-third of the fractions are delivered with the edges of the two x-ray fields coincident with the electron field edge; one-third of the fractions are delivered with one edge of the two x-ray fields 9 mm superior and the other edge 9 mm inferior to the electron field edge; and one-third of the fractions are delivered with the placement of the x-ray field edges reversed.

Total-Scalp Irradiation

Total-scalp irradiation is sometimes necessary in the management of malignancies (e.g., cutaneous lymphoma, melanoma, and angiosarcoma) that present with widespread involvement of the scalp and forehead (64,65). Electron-beam therapy is a practical means of achieving the therapeutic goal of delivering a uniform dose to the scalp with minimal dose to underlying brain. For many years, total-scalp irradiation was achieved by patching multiple electron fields (1,64). Although effective, the treatment was tedious as a result of the large number of fields, their requirement for skin collimation, and the need to move the abutment border to improve dose homogeneity (1). Akazawa (2) from the University of California—San Francisco reported a simpler technique that abuts lateral electron fields to parallel opposed photon fields, the latter of which treats the rind of the scalp avoiding brain tissue. Tung and associates (65) modified the abutment scheme to account for beam divergence and demonstrated improved dose uniformity by comparing 3D dose calculations with *in vivo* dose measurements.

Figure 7.31 illustrates the abutment scheme. The outer edge of the electron field overlaps the inner edge of the 6 MV x-ray field by 3 mm to account for the divergence of the contralateral 6 MV x-ray field. Because the electron and x-ray penumbras are not matched, their common border is moved 1 cm toward beam center halfway through treatment to improve dose homogeneity. Figure 7.32 shows the dose distribution in a transverse CT plane, which illustrates the dose homogeneity achieved in the region of abutment and the sparing of brain tissue. Initially, the common border is set at approximately 0.5 cm inside the inner table of the skull. Moving the common border further toward the inner table of the skull reduces brain irradiation at the expense of the x-ray beam being replaced by an electron beam that would begin to graze the skull. As discussed earlier, grazing radiation penetrates less deeply, possibly underdosing the scalp in this region. Also

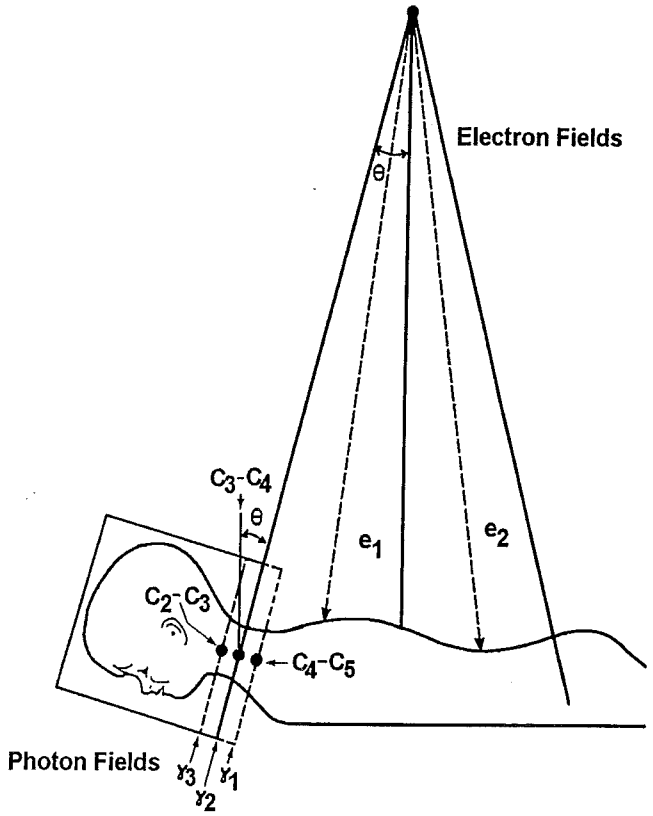

FIGURE 7.29. Schematic of abutment scheme for craniospinal irradiation. Two electron fields are abutted using the common-edge technique to provide homogeneous dose in abutment region in spine. Parallel opposed, lateral, 6-MV x-ray fields used to irradiate brain have a collimator rotation (θ) to align their inferior edge with the superior edge of the electron field. The x-ray field edge is feathered to produce a penumbral shape closely matched to that of the electron beam (41).

noticeable in Fig. 7.32 is a 6-mm thick wax bolus, which increases surface dose for both the electron and x-ray fields.

Total-Limb Irradiation

Occasionally, it is advantageous to irradiate the superficial anatomy of a limb for management of cancer (e.g., melanoma, lymphoma, Kaposi's sarcoma). If the depth beneath the surface is approximately 2 cm or less, then electrons offer a technique of delivering a uniform dose while sparing deep tissues and structures. This technique has been described by Wooden and colleagues (68) for the treatment of the lower calf of a patient with Kaposi's sarcoma. Illustrated in Fig. 7.33, six equally spaced 5-MeV electron beams are used to irradiate a 9-cm diameter cylinder. Each beam is sufficiently wide, so that the entire circle falls within the uniform portion of each beam. Grazing radiation at the edges of the cylinder delivers a greater dose as a result of oblique incidence, which is partially offset by the inverse square effect. Also, the grazing radiation penetrates less deeply. The utilization of six or more beams begins to simulate 360° arc therapy (not possible as a result of patient or table collision). The resulting dose distribution illustrates three significant characteristics. First, the average maximum dose along each radius is approximately 2.55 times the given dose of each of the six fields. Second, 90% of the average maximum dose penetrates 8 to 10 mm, reduced from the value of 15 mm for a single beam incident normally on a flat surface (Fig. 7.26). Third, the surface dose has increased to 90% or greater of average maximum dose compared with approximately 70% of given dose for a single beam incident normally on a flat surface. This is the result of the self-bolusing effect of grazing electron radiation.

One of the challenges of this technique is patient setup and immobilization. Half of the fields are delivered with the patient

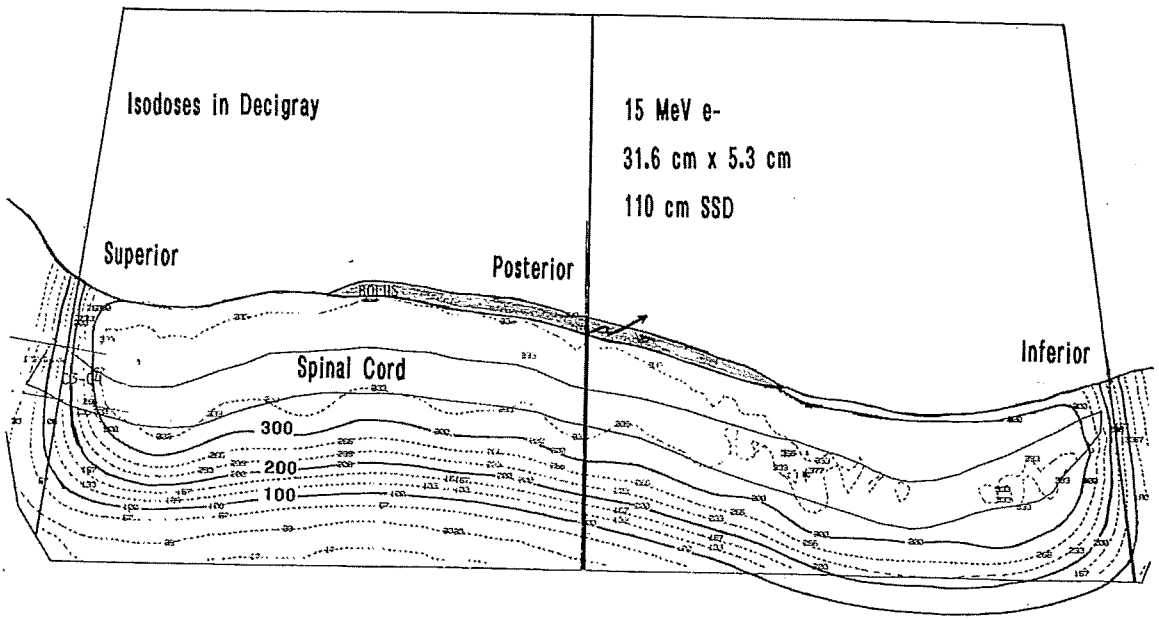

FIGURE 7.30. Electron dose distribution in sagittal plane of spinal field. The penetration of the electron beam is varied using bolus (note taper at edges of bolus to prevent hot or cold spots) to account for variation of the depth of the anterior aspect of the spinal theca. The 30 Gy isodose contour corresponds to 90% of the given dose, and it penetrates approximately 7 mm beyond the spinal cord—4 mm to account for increased energy loss in the bone (dose calculated assuming patient was water) and 3 mm to provide a margin for error (41).

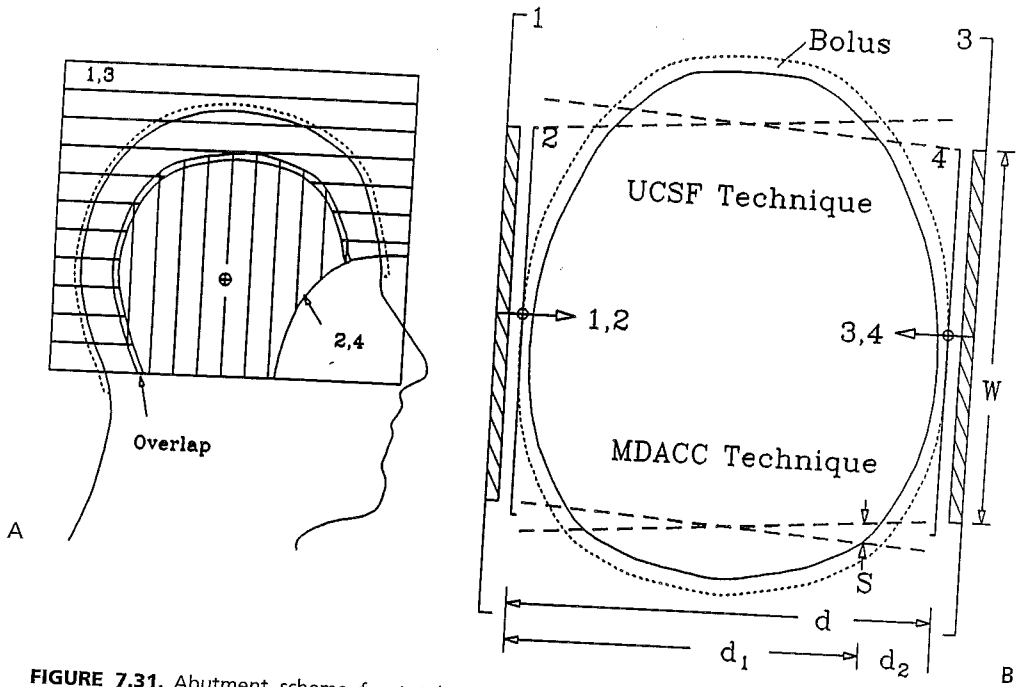

FIGURE 7.31. Abutment scheme for total-scalp irradiation (x-ray fields, 1,3; electron fields, 2,4). **A:** The electron field edge, placed just inside the skull, overlaps the edge of the ipsilateral x-ray field by approximately 3 mm to account for divergence of the edge of the contralateral x-ray field. Halfway through treatment, the field edges are moved 1 cm to improve dose homogeneity in the region of abutment. **B:** The need for the 3-mm overlap (MDACC technique) is better appreciated viewing the divergent edges of all fields in a transverse plane. (From Tung SS, Shiu AS, Starkschall G, et al. Dosimetric evaluation of total scalp irradiation using a lateral electron-photon technique. *Int J Radiat Oncol Biol Phys* 1993;27:153–160, with permission.)

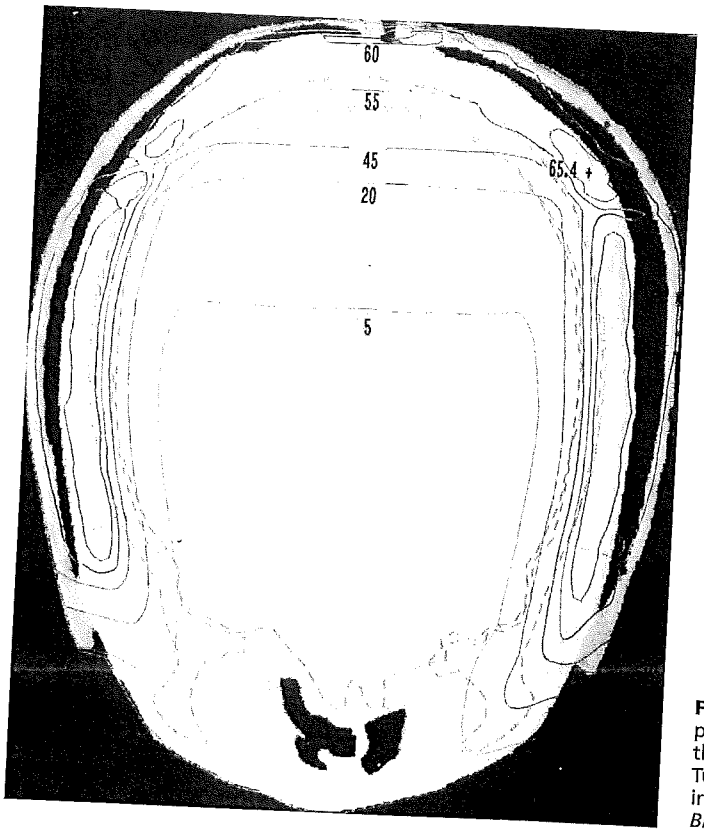

FIGURE 7.32. Dose distribution in a transverse computed tomography plane, illustrating the homogeneity of dose in the abutment region and the degree of brain sparing with this technique. Isodose values in Gy. (From Tung SS, Shiu AS, Starkschall G, et al. Dosimetric evaluation of total scalp irradiation using a lateral electron-photon technique. *Int J Radiat Oncol Biol Phys* 1993;27:153–160, with permission.)

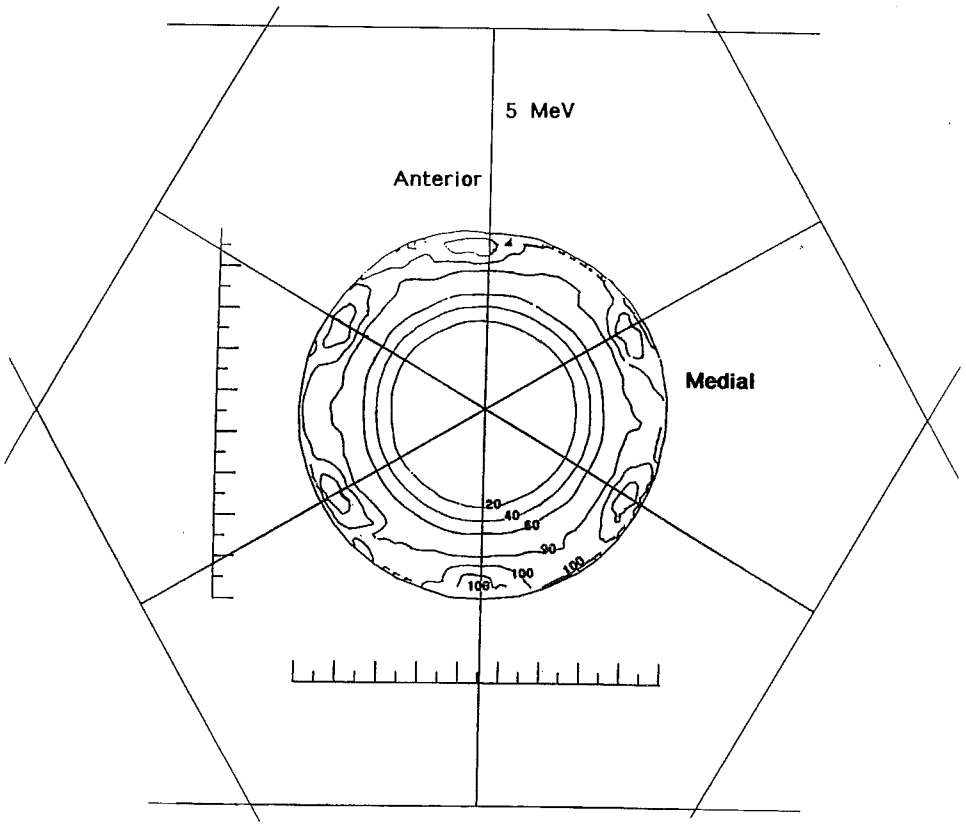

FIGURE 7.33. Dose distribution for total-limb irradiation. Six equally spaced 17-cm wide, 5-MeV electron beams are used to irradiate a 9-cm diameter cylinder. 100% equals 2.55 times the given dose from a single field. (From Wooden KK, Hogstrom KR, Blum P, et al. Whole-limb irradiation of the lower calf using a six-field electron technique. *Med Dosim* 1996;21:211–218, with permission.)

in the prone position and half in the supine position. Also, it might be necessary to deviate slightly from six or eight equally spaced beams to avoid collision of the gantry with the patient or the table. The acceptability of the dose distribution resulting from such variations should be evaluated using one's treatment-planning system.

Total-Skin Irradiation

Total-skin electron irradiation is a modality designed for management of diseases that require irradiation of the entire skin surface or a significant portion of it. The technique is used most frequently for treatment of mycosis fungoides, whose management is reviewed by Hoppe (29).

Multiple techniques for total-skin electron therapy have been reviewed in AAPM Report No. 23 (31) and by Almond (3). The underlying principles of the various techniques are all similar, which are exemplified by the modified Stanford technique, illustrated in Fig. 7.34. First, the treatment requires a broad beam from right to left, which can be achieved by a combination of treating the patient at an extended SSD (3 to 4 m) and using an external scattering foil to further broaden the beam. The beam is made uniform from head to foot by abutting two fields at the 50% off-axis ratio (Fig. 7.34A). (Note that the 50% off-axis ratio lies outside the edge of the light field, so when properly abutted, there is a gap of tens of centimeters between the edges of the respective light fields.) By aiming the beams up and down, much of the contaminating bremsstrahlung dose misses the patient. The dose is made uniform around the circumference of the patient by irradiating from six different directions (Fig. 7.34B). Similar to total-limb irradiation, the grazing radiation results in a higher surface dose and a less penetrating dose. Placed upstream of the patient is a 3/8″ plastic plate that serves as both an energy degrader and a scatterer. Scattered electrons increase dose in anatomy obscured by direct line of sight. Dose homogeneity is also dependent on patient position, and reproducing the positions of the Stanford technique (Fig. 7.34C) is important. Despite efforts to create a homogeneous dose, there always will be areas that are underdosed (e.g., top of scalp, sole of feet, perineum, and under the breast or under the panniculus of obese individuals). These areas and sometimes tumorous lesions require separate treatment and boosting, respectively. In contrast, fingers, feet, and toes typically receive excess dose and are shielded for a portion of the treatment. *In vivo* measurement of patient dose on an individual basis is important to making decisions on prescriptions for supplemental treatments, and a report by Antolak and colleagues (4) summarizes the results of *in vivo* dosimetry on patients treated using the modified Stanford technique at M.D. Anderson Cancer Center.

Implementation of this technique is complex. It requires an external patient stand with a plastic diffuser, an external scattering foil to broaden the beam, special dosimetry equipment for quality assurance and calibration, special shields for selected parts of the patient, and access to *in vivo* dosimetry. It is also necessary for the radiation therapy accelerator to have a high–dose-rate mode and interlocks for electron energy, gantry angle, x-ray jaws, and insertion of secondary foil. Despite its technical complexity, it remains somewhat of an art. This factor coupled

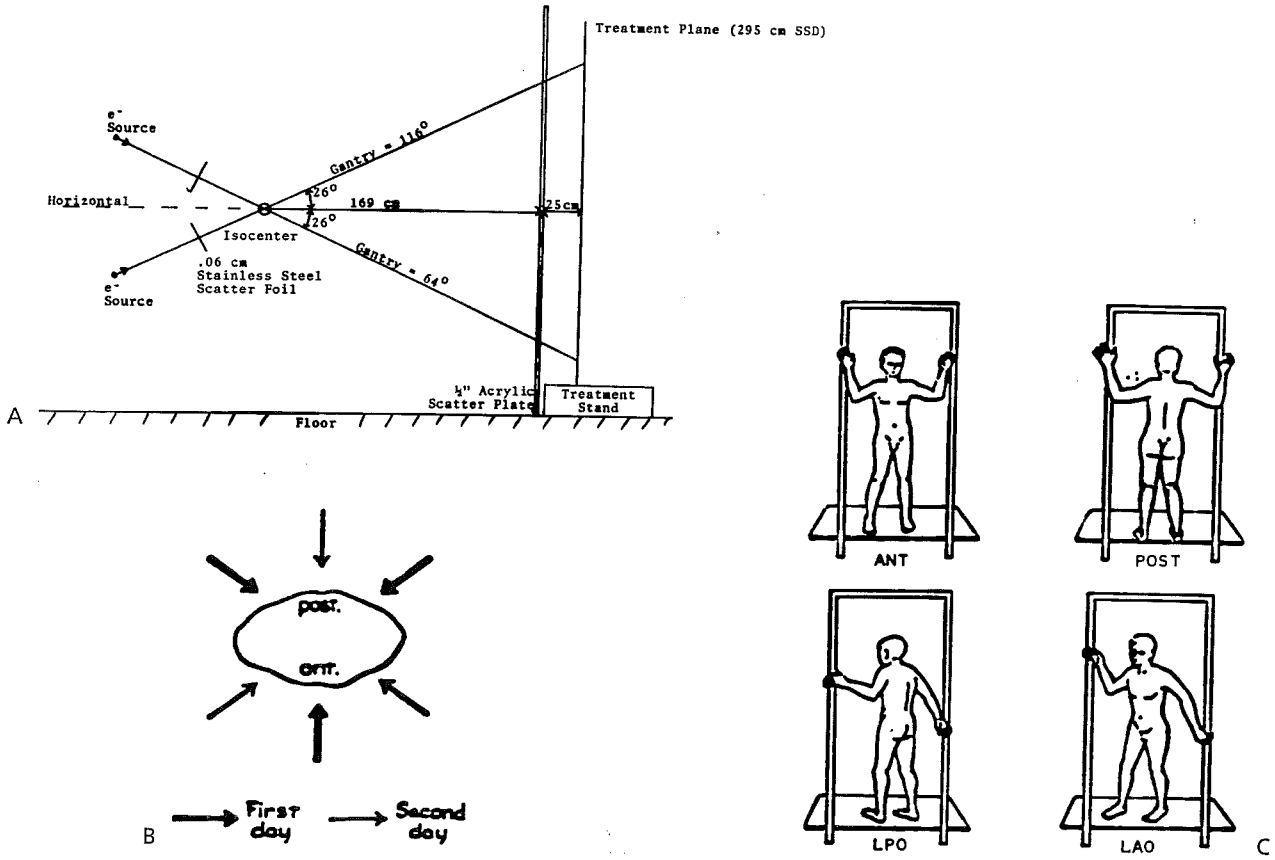

FIGURE 7.34. Schematic of modified Stanford technique. **A:** Side view of setup shows the relative position of patient plane, scatter plate, isocenter, and gantry angles. **B:** Six beam directions are achieved by placing patient in **(C)** six patient positions. (From Almond, PR. Total skin electron irradiation technique and dosimetry. In: Kereiakes JG, Elson HR, Born CG, eds. *Radiation Oncology Physics 1986.* New York: American Institute of Physics, Inc., 1987:296–332 and Karzmark CJ, Anderson J, Fessenden P, et al. *AAPM Report No. 23, total skin electron therapy: technique and dosimetry.* New York: American Institute of Physics, Inc., 1987, with permission.)

with the low incidence of its use emphasizes the need for the radiation oncologist and medical physicist to be experienced in this technique.

Electron Arc Therapy

Electron arc therapy is useful for treating postmastectomy chest wall (24,63). It is used in lieu of parallel-opposed tangential photon irradiation. It is more useful in barrel-chested women, where tangent beams can irradiate too much lung. It is also difficult to achieve homogeneous dose in the region where the tangent beams used for the chest wall abut the anterior beam use for the internal mammary chain, which is a problem if disease is present there. In such cases, treating both areas with only opposed tangent photon beams irradiates too much lung, so in such cases electron arc therapy is a viable option. This can be particularly important in patients with bilateral disease.

The treatment geometry and dosimetry for arc therapy are unique and are discussed in detail by Hogstrom and Leavitt (24). There are three levels of collimation in electron arc therapy: the primary x-ray collimators, a shaped secondary Cerrobend insert, and skin collimation (Fig. 7.35). The secondary collimator typically projects a 5- to 6-cm beam width at isocenter. There is typically a large air gap between the secondary collimating insert and the patient, resulting in a large penumbra; also, the finite width of the field results in a broad edge at the end of the arc. The sharpness of the penumbra is restored utilizing skin collimation. This requires that the edge of the field of the secondary collimator extend well beyond the edge of the field defined by skin collimation. In the plane of rotation, this is achieved by rotating approximately 15° beyond the treatment field edge (Fig. 7.36).

As previously discussed, depth dose for an arced beam differs from that for a fixed beam (Fig 7.26B); the surface dose is significantly less and the dose fall-off becomes slightly sharper. Consequently, bolus may be required to deliver adequate dose superficially. Another consequence of arcing is that a constant width of the secondary collimator results in dose inhomogeneity in the cephalocaudal direction. The radius of curvature of the patient with respect to the accelerator isocentric axis is typically less superiorly, as the neck is approached. If the radius of curvature is less, then the skin is further from the electron source (i.e., a greater SSD). Contrary to fixed-beam therapy, the dose to that region increases rather than decreases as a result of focusing of the electron fluence towards isocenter (24); however, by reducing the collimator width, the dose can be made more uniform.

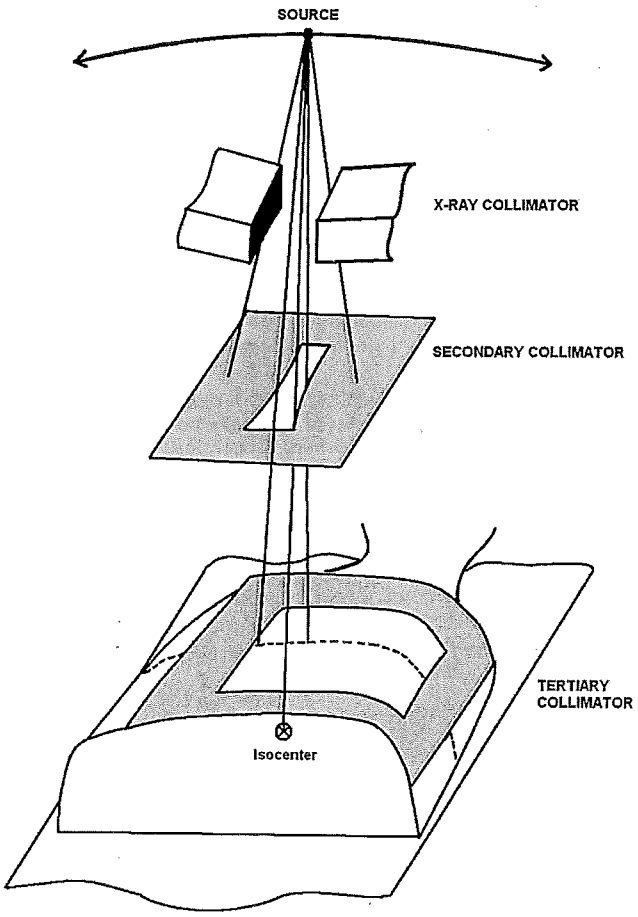

FIGURE 7.35. Schematic of treatment geometry for electron arc therapy. Skin collimation is required because of the large air gap between secondary collimator and patient, which is needed to allow rotation of the gantry around the patient.

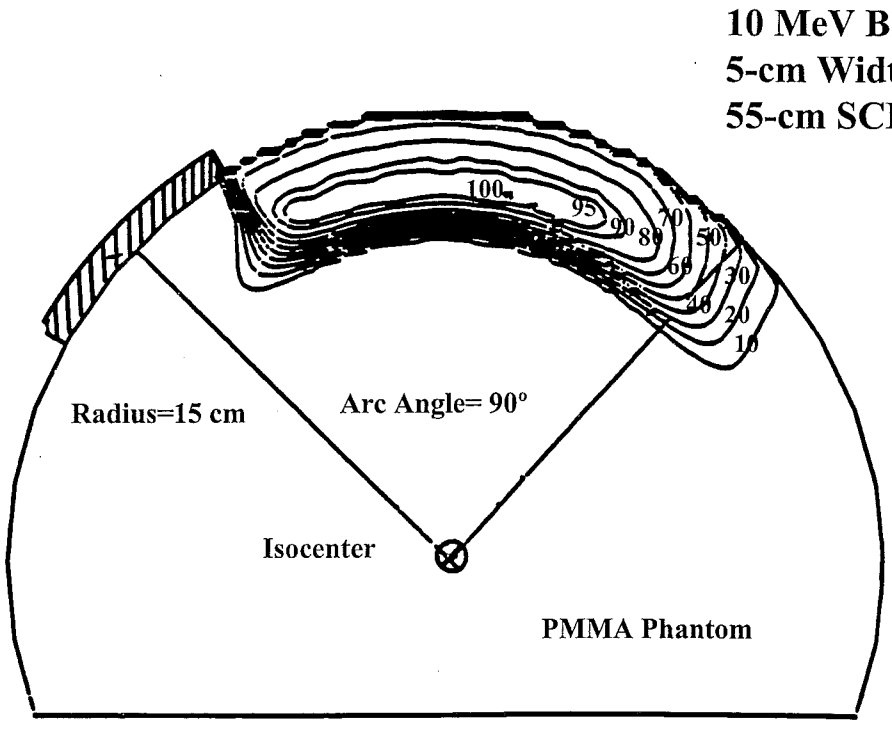

FIGURE 7.36. Comparison of dose distribution with and without skin collimation. The uncollimated edge has a slow dose fall-off that is useful for abutting to other arced fields. The skin collimation restores the beam edge but requires rotating the beam 15° beyond the edge of the skin collimator.

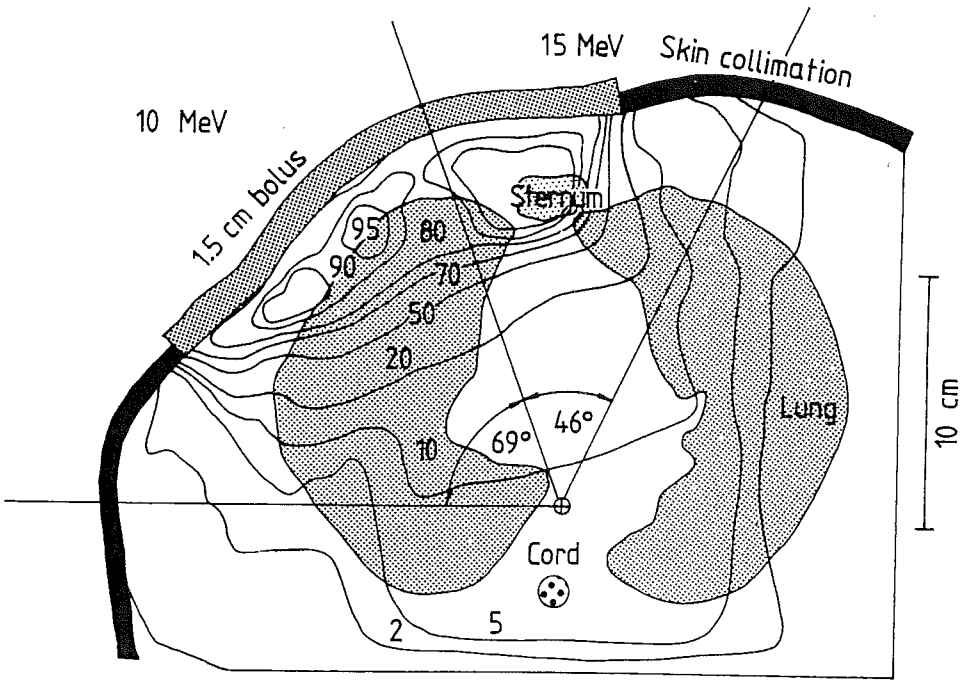

FIGURE 7.37. Typical dose distribution achieved by arc electron therapy. Note (a) the different energies used for the IMC and chest-wall fields, (b) the exact abutment of the IMC and chest-wall fields, (c) the rotation 15° beyond the skin edges of the skin collimator, and (d) the use of bolus to increase the surface dose. (From Hogstrom KR, Kurup RG, Shiu AS, et al. A two-dimensional pencil-beam algorithm for calculation of arc electron dose distributions. *Phys Med Biol* 1989;34:315–341, with permission.)

The treatment-planning process for arc therapy requires patient CT scanning, delineation of PTV, selection of isocenter location, specification of electron arc boundaries, energy and slab bolus selection, design of secondary collimator, and calculation of dose (23) and monitor units (24). Figure 7.37 shows a typical dose distribution that can be achieved using arc therapy for irradiation of the internal mammary chain and chest wall.

SUMMARY

Electron-beam therapy remains an important modality to the practice of radiation therapy. As discussed earlier, its effective use requires knowledge of the unique properties of electron-beam dose distributions, the impact of the patient on the dose distribution, and the basic principles for good practice. It requires access to and the proper use of comprehensive treatment planning and delivery tools. It also requires access to special techniques that offer unique treatment solutions for a limited number but broad range of patient conditions.

Electron therapy can be expected to become more sophisticated in the future as the enthusiasm for intensity-modulated radiation therapy will carry into electron therapy. Advances in electron dose calculations, methods for electron-beam optimization, and availability of electron multileaf collimators will enable the practice of intensity-modulated and energy-modulated electron therapy. This will advance both electron conformal and mixed-beam therapy.

REFERENCES

1. Able CM, Mills MD, McNeese MD, et al. Evaluation of a total scalp electron irradiation technique. *Int J Radiat Oncol Biol Phys* 1991;21:1063–1072.
2. Akazawa C. Treatment of the scalp using photon and electron beams. *Med Dosim* 1989;14:129–131.
3. Almond, PR. Total skin electron irradiation technique and dosimetry. In: Kereiakes JG, Elson HR, Born CG, eds. *Radiation Oncology Physics 1986.* New York: American Institute of Physics, Inc., 1987:296–332.
4. Antolak JA, Cundiff JH, Ha CS. Utilization of thermoluminescent dosimetry in total skin electron beam radiation therapy of mycosis fungoides. *Int J Radiat Oncol Biol Phys* 1998;40:101–108.
5. Biggs PJ, Boyer AL, Doppke KP. Electron dosimetry of irregular fields on Clinac-18. *Int J Radiat Oncol Biol Phys* 1979;5:433–440.
6. Biggs PJ, Wang CC. Breakaway safety feature for an intra-oral cone system. *Int J Radiat Oncol Biol Phys* 1984;10:1117–1119.
7. Boyd RA, Hogstrom KR, Antolak JA, et al. A measured data set for evaluating electron-beam dose algorithms. *Med Phys* 2001;28:950–958.
8. Boyd RA, Hogstrom KR, Rosen II. Effect of using an initial polyenergetic spectrum with the pencil-beam redefinition algorithm for electron-dose calculations in water. *Med Phys* 1998;25:2176–2185.
9. Boyd RA, Hogstrom KR, and Starkschall G. Electron pencil-beam redefinition algorithm dose calculations in the presence of heterogeneities. *Med Phys* 2001;28:2096–2104.
10. Dewit L, Van Dam J, Rijnders A, et al. A modified radiation therapy technique in the treatment of medulloblastoma. *Int J Radiat Oncol Biol Phys* 1984;10:231–241.
11. Dominiak GS. *Dose in spinal cord following electron irradiation.* The University of Texas Health Science Center at Houston, Graduate School of Biomedical Sciences, 1991.
12. Donaldson SS, Findley DO. Treatment of orbital lymphoid tumors with electron beams. In: Vaeth JM, Meyer JL, eds. *Frontiers of Radiation Therapy and Oncology Vol. 25: The Role of High Energy Electrons in the Treatment of Cancer.* Basel: S. Karger AG, 1991:187–200.
13. Ekstrand KE, Dixon RL. The problem of obliquely incident beams in electron-beam treatment planning. *Med Phys* 1982;9:276–278.
14. Fields RS, Hogstrom KR. Optimization of Electron-Photon Mixed Beam Planning. In: *Proceedings of the Eight International Conference on the Use of Computers in Radiation Therapy.* Silver Spring: IEEE Computer Society Press, 1984:248–254.
15. Hogstrom KR. Implementation of CT treatment planning. In: Wright AE, Boyer AL, eds. *Advances in Radiation Therapy Treatment Planning.* New York: American Institute of Physics, Inc., 1983:268–281.

16. Hogstrom KR. Dosimetry of electron heterogeneities. In: Wright AE, Boyer AL, eds. *Advances in Radiation Therapy Treatment Planning.* New York: American Institute of Physics, Inc., 1983:223–243.
17. Hogstrom, KR. Evaluation of electron pencil beam dose calculations. In: Kereiakes JG, Elson HR, Born CG, eds. *Radiation Oncology Physics 1986.* New York: American Institute of Physics, Inc., 1987:532–557.
18. Hogstrom, KR. Clinical electron beam dosimetry: basic dosimetry data. In: Purdy JA, ed. *Advances in Radiation Oncology Physics: Dosimetry, Treatment Planning, and Brachytherapy.* Woodbury: American Institute of Physics, Inc., 1991:390–429.
19. Hogstrom KR. Treatment planning in electron beam therapy. In: Vaeth JM, Meyer JL, eds. *Frontiers of Radiation Therapy and Oncology Vol. 25: The Role of High Energy Electrons in the Treatment of Cancer.* Basel: S. Karger AG, 1991:30–52.
20. Hogstrom KR, Boyer AL, Shiu AS, et al. Design of metallic electron beam cones for an intraoperative therapy linear accelerator. *Int J Radiat Oncol Biol Phys* 1990;18:1223–1232.
21. Hogstrom KR, Fields RS. Use of CT in electron beam treatment planning: current and future development. In: Ling CC, Rogers CC, Morton RJ, eds. *Computed Tomography in Radiation Therapy,* New York: Raven Press, 1983:241–252.
22. Hogstrom KR, Horton JL, Kutcher GJ, et al. *ACMP Task Group Report: Survey of Physics Resources for Radiation Oncology Special Procedures.* Reston: American College of Medical Physics, 1998.
23. Hogstrom KR, Kurup RG, Shiu AS, et al. A two-dimensional pencil-beam algorithm for calculation of arc electron dose distributions. *Phys Med Biol* 1989;34:315–341.
24. Hogstrom KR, Leavitt D. Dosimetry of electron arc therapy. In: Kereiakes JG, Elson HR, Born CG, eds. *Radiation Oncology Physics 1986.* New York: American Institute of Physics, 1987:265–295.
25. Hogstrom KR, Mills MD, Almond PR. Electron beam dose calculations. *Phys Med Biol,* 1981;26:445–459.
26. Hogstrom KR, Mills MD, Meyer JA, et al. Dosimetric evaluation of a pencil-beam algorithm for electrons employing a two-dimensional heterogeneity correction. *Int J Radiat Oncol Biol Phys* 1984;10:561–569.
27. Hogstrom KR, Steadham RE. Electron beam dose computation. In: Palta JR, Mackie TR, eds. *Teletherapy: Present and Future.* Madison: Advanced Medical Publishing, 1996:137–174.
28. Hogstrom, KR, Steadham RE, Wong PF, et al. Monitor unit calculations for electron beams. In: Gibbons JP, ed. *Monitor Unit Calculations for External Photon and Electron Beams.* Madison: Advanced Medical Publishing, Inc., 2000:113–126.
29. Hoppe, RT. Total skin electron beam therapy in the management of mycosis fungoides. In: Vaeth JM, Meyer JL, eds. *Frontiers of Radiation Therapy and Oncology Vol. 25: The Role of High Energy Electrons in the Treatment of Cancer.* Basel: S. Karger AG, 1991:80–89.
30. ICRU Report 35. *Radiation dosimetry: Electron beams with energies between 1 and 50 MeV.* Bethesda: International Commission on Radiation Units and Measurement, 1984.
31. Karzmark CJ, Anderson J, Fessenden P, et al. *AAPM Report No. 23, total skin electron therapy: technique and dosimetry.* New York: American Institute of Physics, Inc., 1987.
32. Khan FM. *The Physics of Radiation Therapy, 2nd ed.* Baltimore: Lippincott Williams & Wilkins, 1994.
33. Khan FM, Doppke KP, Hogstrom KR, et al. Clinical electron-beam dosimetry: Report of AAPM Radiation Therapy Committee Task Group No. 25. *Med Phys* 1991;18:73–109.
34. Kirsner SM, Hogstrom KR, Kurup RG, et al. Dosimetric evaluation in heterogeneous tissue of anterior electron beam irradiation for treatment of retinoblastoma. *Med Phys* 1987;14:772–779.
35. Klevenhagen SC, Lambert GD, Arbabi A. Backscattering in electron beam therapy for energies between 3 and 35 MeV. *Phys Med Biol* 1982;27:363–373.
36. Kudchadker RJ, Hogstrom KR, Garden AS, et al. Electron conformal radiation therapy using bolus and intensity modulation. *Int J Radiat Oncol Biol Phys* 2002;53:1023–1037.
37. Kun LE. Electron beam therapy in children. In: Vaeth JM, Meyer JL, eds. *Frontiers of Radiation Therapy and Oncology Vol. 25: The Role of High Energy Electrons in the Treatment of Cancer.* Basel: S. Karger AG, 1991:201–206.
38. Lambert GD, Klevenhagen SC. Penetration of backscattered electrons in polystyrene for energies between 1 and 25 MeV. *Phys Med Biol* 1982;27:721–725.
39. Low DA, Starkschall G, Bujnowski SW, et. al. Electron bolus design for radiation therapy treatment planning: Bolus design algorithms. *Med Phys* 1992;19:115–124.
40. Low DA, Starkschall G, Sherman NE, et al. Computer-aided design and fabrication of an electron bolus for treatment of the paraspinal muscles. *Int J Radiat Oncol Biol Phys* 1995;33:1127–1138.
41. Maor MH, Fields RS, Hogstrom KR, et al. Improving the therapeutic ratio of craniospinal irradiation in medulloblastoma. *Int J Radiat Oncol Biol Phys* 1985;11:687–697.
42. Maor MH, Hogstrom KR, Fields RS, et al. Newer approaches to cerebrospinal irradiation in pediatric brain tumors. In: Brooks BF, ed. *Malignant Tumors of Childhood.* Austin: The University of Texas Press, 1986:245–254.
43. McGinnis WL, Bischof CJ, Latourette HB. Transvaginal cone electron beam technique for a Varian 18 MeV linear accelerator. *Int J Radiat Oncol Biol Phys* 1979;5:123–125.
44. Merrick HW III, Dobelbower RR Jr, Konski AA. Intraoperative radiation therapy for pancreatic, biliary and gastric carcinoma: the US experience. In: Vaeth JM, Meyer JL, eds. *Frontiers of Radiation Therapy and Oncology Vol. 25: The Role of High Energy Electrons in the Treatment of Cancer.* Basel: S. Karger AG, 1991:246–257.
45. Meyer JA, Palta JR, Hogstrom KR. Demonstration of relatively new electron dosimetry measurement techniques on the Mevatron 80. *Med Phys* 1984;11:670–677.
46. Million RR, Parson JT, Bova FJ, et al. Electron beam: the management of head and neck cancer. In: Vaeth JM, Meyer JL, eds. *Frontiers of Radiation Therapy and Oncology Vol. 25: The Role of High Energy Electrons in the Treatment of Cancer.* Basel: S. Karger AG, 1991:107–127.
47. Mills MD, Fuller LM, Zagars GK, et al. Spinal cord dose reduction using an anterior 13 MeV electron field situated between a split anterior ^{60}Co supraclavicular field. *Int J Radiat Oncol Biol Phys* 1987;13:1571–1575.
48. Mills MD, Hogstrom KR, Almond PR. Prediction of electron beam output factors. *Med Phys* 1982;9:60–68.
49. Mills MD, Hogstrom KR, Fields RS. Determination of electron beam output factors for a 20-MeV linear accelerator. *Med Phys* 1985;12:473–476.
50. Morrison WH, Wong PF, Starkschall G, et al. Water bolus for electron irradiation of the ear canal. *Int J Radiat Oncol Biol Phys* 1995;33:479–483.
51. Nyerick CE, Ochran TG, Boyer AL, et al. Dosimetry characteristics of metallic cones for intraoperative radiation therapy. *Int J Radiat Oncol Biol Phys* 1991;21:501–510.
52. Perez CA. Management of vulvar cancer. In: Vaeth JM, Meyer JL, eds. *Frontiers of Radiation Therapy and Oncology Vol. 25: The Role of High Energy Electrons in the Treatment of Cancer.* Basel: S. Karger AG, 1991:183–186.
53. Perkins GH, McNeese MD, Antolak JA, et al. A custom three-dimensional electron bolus technique for optimization of postmastectomy irradiation. *Int J Radiat Oncol Biol Phys* 2001;51:1142–1151.
54. Perry DJ, Holt JG. A model for calculating the effects of small inhomogeneities on electron beam dose distributions. *Med Phys* 1980;7:207–215.
55. Recht A, Triedman SA, Harris JR. The "boost" in the treatment of early-stage breast cancer: electrons versus interstitial implants. In: Vaeth JM, Meyer JL, eds. *Frontiers of Radiation Therapy and Oncology Vol. 25: The Role of High Energy Electrons in the Treatment of Cancer.* Basel: S. Karger AG, 1991:169–179.
56. Shiu AS, Hogstrom KR. Dose in bone and tissue near bone-tissue interface from electron beam. *Int J Radiat Oncol Biol Phys* 1991;21:695–702.
57. Shiu AS, Hogstrom KR. Pencil-beam redefinition algorithm for electron dose distributions. *Med Phys* 1991;18:7–18.
58. Shiu AS, Tung SS, Gastorf RJ, et al. Dosimetric evaluation of lead and tungsten eye shields in electron beam treatment. *Int J Radiat Oncol Biol Phys* 1996;35:599–604.

59. Shiu AS, Tung S, Hogstrom KR, et al. Verification data for electron beam dose algorithms. *Med Phys* 1992;19:623–636.
60. Shiu AS, Tung SS, Nyerick CE, et al. Comprehensive analysis of electron beam central axis dose for a radiation therapy linear accelerator. *Med Phys* 1994;21:559–566.
61. Starkschall G, Antolak JA, Hogstrom KR. Electron beam bolus for 3-D conformal radiation therapy. In: Purdy JA, Emami B, eds. *3-D Radiation Treatment Planning and Conformal Therapy, Proceedings of an International Symposium.* Madison: Medical Physics Publishing, 1995:265–282.
62. Starkschall G, Shiu AS, Bujnowski SW, et al. Effect of dimensionality of heterogeneity corrections on the implementation of a three-dimensional electron pencil-beam algorithm. *Phys Med Biol* 1991;36:207–227.
63. Stewart JR, Leavitt DD, Prows J. Electron arc therapy of the chest wall for breast cancer: rationale, dosimetry, and clinical aspects. In: Vaeth JM, Meyer JL, eds. *Frontiers of Radiation Therapy and Oncology Vol. 25: The Role of High Energy Electrons in the Treatment of Cancer.* Basel: S. Karger AG, 1991:134–150.
64. Tapley ND, ed. *Clinical Applications of the Electron Beam.* New York: John Wiley & Sons, Inc., 1976.
65. Tung SS, Shiu AS, Starkschall G, et al. Dosimetric evaluation of total scalp irradiation using a lateral electron-photon technique. *Int J Radiat Oncol Biol Phys* 1993;27:153–160.
66. Vaeth JM, Meyer JL, eds. *Frontiers of Radiation Therapy and Oncology Vol. 25: The Role of High Energy Electrons in the Treatment of Cancer.* Basel: S. Karger AG, 1991.
67. Wang, CC. Intraoral cone for carcinoma of the oral cavity. In: Vaeth JM, Meyer JL, eds. *Frontiers of Radiation Therapy and Oncology Vol. 25: The Role of High Energy Electrons in the Treatment of Cancer.* Basel: S. Karger AG, 1991:128–131
68. Wooden KK, Hogstrom KR, Blum P, et al. Whole-limb irradiation of the lower calf using a six-field electron technique. *Med Dosim* 1996;21:211–218.